University of São Paulo
"Luiz de Queiroz" College of Agriculture

Depth images' processing to improve the performance of sows through early
detection of lameness and changes in body condition score

Isabella Cardoso Ferreira da Silva Condotta

Thesis presented to obtain the degree of Doctor of
Science. Area: Agricultural Systems Engineering

Piracicaba
2019

Isabella Cardoso Ferreira da Silva Condotta
Agricultural Engineer
Licentiate in Agricultural Sciences

Depth images' processing to improve the performance of sows through early detection of lameness and changes in body condition score

versão revisada de acordo com a resolução CoPGr 6018 de 2011

Advisor
Prof. Dr. **KÉSIA OLIVEIRA DA SILVA-MIRANDA**

Thesis presented to obtain the degree of Doctor of Science. Area: Agricultural Systems Engineering

Piracicaba
2019

DEDICATORY

To my dear mother, from whom I have always had unconditional love and support, and whose steps I have been following, so that today I could learn to fly;

I dedicate

AKNOWLEDGEMENTS

To Prof. Késia Oliveira da Silva Miranda, for her contribution in my academic education and guidance in the last nine years;

To Prof. Tami M. Brown-Brandl, for all the guidance, friendship and welcome during my stay in the United States;

To my professors and members of my committee, Dr. Aérica Cirqueira Nazareno, Prof. Cesar Gonçalves de Lima, Prof. Daniella Jorge de Moura, Prof. Hae Yong Kim, Prof. Idemauro Antonio Rodrigues de Lara, Prof. Iran José Oliveira da Silva, Prof. Jorge Lizardo Diaz Calle, Prof. Marcelo Andrade da Costa Vieira, Prof. Marcelo Becker, Prof. Roseli Aparecida Leandro, and Prof. Urbano dos Santos Ruiz. Thank you for the guidance and suggestions;

To GBAZP group and its students (Caroline, Daniel, Daniele, Felipe, Laís, Luana, and Tássio), that provided me with experience on both learning and teaching, and the basis for doing good research;

To the USMARC people for all the support and the working environment provided, specially to John, for playing cards during lunch; Mindy, for the fun rides; and Bryan, for teaching my husband how to tease on me;

To the USMARC swine facility personnel, that provided the support necessary to collect my data;

To the Brandl's family and to the friends from Aurora-NE, especially Barb, that had an important role on making life more fun during the last year;

To "nachos", old friends with whom I celebrate the international muffin day (18/12, for those who do not know) to eternalize our friendship. Especially to Marina (or Thainá Ribeiro, as you prefer), who has been always by my side, even when I am far away;

To "Fast Family", my crazy family of athletes (some not so much) that, to this day, do not know in which city I live and what is my major, but that always accompany me and vibrate with my achievements;

To my father, Artur Condotta, who, in his own way, has always supported me and who teaches me, in broken ways, the importance of forgiveness;

To my in-laws, Ana and Claudemir de Oliveira, who allowed me to be part of their family and entrusted me their most precious possession;

To Lu (Luciano de Oliveira), my beloved husband, that gives me support and motivation, even in the darkest moments, and plays a fundamental role so that I can see life in a more colorful way. You are the one that sees my true colors, and I know that, if I call you up, you'll always be there;

To my mother, Marilene Cardoso, to whom I dedicate this work; without you I would not exist (really) and would not be half the person I am;

To all those who have contributed in some way to my development both as a professional and as a person, and to the progress of this project;

To God, who is always with me, even when I forget it.

Thank you very much!

EPIGRAPH

For I know the plans I have for you, declares the Lord, plans to prosper you and not to harm you, plans to give you hope and a future. Then you will call on me and come and pray to me, and I will listen to you. You will seek me and find me when you seek me with all your heart.

-Jeremiah 29:11-13

"Logic will get you from A to B. Imagination will get you everywhere."

-Albert Einstein

CONTENTS

RESUMO

Processamento de imagens em profundidade para melhora do desempenho de matrizes suínas por meio da detecção precoce de claudicação e de alterações no escore de condição corporal

A observação, o controle e a manutenção das condições físicas de matrizes suínas em níveis aceitáveis são fundamentais para manter o bem-estar animal e a produção em padrões adequados. A claudicação causa dor e dificuldade de locomoção e, no entanto, é uma desordem comum em matrizes suínas que, além do impacto negativo no bem-estar, gera, também, grandes impactos na produção, uma vez que os animais que demonstram esse problema, apresentam um menor número de leitões nascidos vivos, menor número de partos por ano e são removidas do rebanho a uma idade mais jovem do que a ideal. Sabe-se, ainda, que, durante a gestação, cada matriz deve receber uma quantidade de ração diferenciada de acordo com sua condição corporal. Animais abaixo do peso apresentam deficiência nutricional e menor número de leitões nascidos por ninhada. Já as matrizes com excesso de peso apresentam um desenvolvimento anormal das glândulas mamárias, reduzindo a quantidade de leite produzida durante a lactação, acarretando em perdas econômicas. Tanto a detecção da claudicação quanto a classificação da condição corporal são feitos por meios subjetivos e dependentes da opinião pessoal do tratador, o que pode gerar divergências entre as classificações dadas por cada indivíduo. Destaca-se, portanto, a importância do reconhecimento precoce de animais que apresentam condições físicas fora dos padrões exigidos, visando a prevenção de perdas produtivas causadas tanto pelo agravamento das condições apresentadas quanto pelo grande impacto no bem-estar dos animais. Tendo-se isso em vista, o presente trabalho visou obter três características (escore de condição corporal, massa corporal e espessura de toucinho) por meio de imagens em profundidade, que se mostraram eficazes na obtenção dessas características em outros animais (suínos machos não-castrados e vacas leiteiras). Além disso, buscou-se desenvolver um método para a detecção precoce de claudicação em matrizes suínas, utilizando-se a abordagem da cinemática dos animais, que vem dando bons resultados e cujas dificuldades têm potencial para serem sanadas por meio do uso de imagens em profundidade em vez do método de marcadores reflexivos utilizado atualmente. Para predizer a condição corporal, uma regressão linear múltipla foi obtida usando o menor eixo da elipse ajustada ao redor do corpo da matriz suína, a largura dos ombros e o ângulo da curvatura da última costela. Para predizer a espessura de toucinho, foi realizada uma regressão linear múltipla usando a altura curvatura da última da costela, o perímetro do corpo da matriz, o maior eixo da elipse ajustada, o comprimento do focinho à cauda e o escore predito da condição corporal. Foi possível obter a massa corporal com uma regressão linear simples usando o volume projetado do corpo das matrizes. Para detecção de claudicação, três modelos apresentaram a melhor precisão (76,9%): análise discriminante linear, 1 vizinho mais próximo e 10 vizinhos mais próximos. As variáveis de entrada utilizadas nos modelos foram obtidas a partir de vídeos em profundidade (número, tempo e comprimento de passos para cada uma das quatro regiões analisadas-ombros esquerdo e direito e quadris esquerdo e direito; tempo total de caminhada e número de máximos locais para a região da cabeça). Como resultado desses estudos, observou-se que câmeras em profundidade podem ser utilizadas na automação de medidas de peso, condição corporal, espessura de toucinho e claudicação de matrizes suínas.

Palavras-chave: Zootecnia de precisão; Bem-estar; Tempo de voo, Dimensões

ABSTRACT

Depth images' processing to improve the performance of sows through early detection of lameness and changes in body condition score

The observation, control and the maintenance of the physical condition of sows in acceptable levels are critical to maintain the animal welfare and production in appropriate standards. Lameness causes pain making locomotion difficult. However, lameness is a common disorder in sows that causes negative impacts in both welfare and production. Since the animals that demonstrate this problem, have a smaller number of born-alive piglets, fewer gestation per year and are removed from the herd at a younger age than the ideal. In addition, it is industry practice to limit feed sows to ensure that they remain at an ideal condition score. It is known that, during gestation, each sow should receive a different amount of food according to its body condition. Underweight animals have nutritional deficiency and lower number of piglets per litter. On the other hand, overweight sows have an abnormal development of mammary glands, reducing the amount of milk produced during lactation, causing economic losses. However, moving sows to group gestation makes it difficult to monitor condition score in gestating sows. Both the detection of lameness and the classification of body condition are currently assessed using subjective methods, which is time consuming and difficult to accurately complete. Therefore, the early recognition of animals that present physical condition outside the standards is important to prevent production losses caused by both the aggravation of the conditions presented and the impact on the animals' welfare. The objective of this project is to obtain three characteristics (body condition score, mass and backfat thickness) through depth images, that proved to be effective on the acquisition of these features in other animals (boars and cows). The second objective is to develop a method for early detection of lameness using the kinematic approach, that has been generating good results and which difficulties have the potential to be reduced by using depth images instead of the method of reflective markers currently used. To predict body condition, a multiple linear regression was obtained using the minor axis of the ellipse fitted around sow's body, the width at shoulders, and the angle, of the last rib's curvature. To predict backfat, a multiple linear regression was performed using the height of last rib's curvature, the perimeter of sow's body, the major axis of the ellipse fitted around sow's body, the length from snout to rump, and the predicted body condition score. It was possible to obtain the body mass with a simple linear regression using the projected volume of the sows' body. For lameness detection, three models presented the best accuracy (76.9%): linear discriminant analysis, fine 1-nearest neighbor, and weighted 10-nearest neighbors. The input variables used on the models were obtained from depth videos (number, time, and length of steps for each of the four regions analyzed - left and right shoulders and left and right hips; total walk time; and number of local maxima for head region). As a result of these studies, it has been demonstrated that a depth camera can be used to automate the weight, condition score, backfat thickness, and lameness acquisition/detection in gestating and lactating sows.

Keywords: Precision livestock farming; Well-being; Time-of-flight; Dimensions

1 INTRODUCTION

The observation, control and maintenance of the physical condition of sows in acceptable levels are critical to maintain the animal welfare and production in appropriate standards. The animal welfare includes its physical and mental state. In December of 1979, it was proposed in the United Kingdom, during the Farm Animal Welfare Council, that the welfare of an animal should be considered in terms of "five freedoms". These freedoms define ideal states rather than acceptable welfare standards (Table 1). Sometimes, a single problem can affect more than one of those freedoms.

Table 1. The five freedoms and their provisions. Adapted from UK Government Web Archive.

Freedom	Provision
Freedom from hunger, thirst and malnutrition	Ready access to fresh water and a diet to maintain full health and vigor
Freedom from discomfort	Appropriate environment including shelter and a comfortable resting area
Freedom from pain, injury or disease	Prevention or rapid diagnosis and treatment
Freedom to express normal behavior	Sufficient space, proper facilities and company of the animal's own kind
Freedom from fear and distress	Conditions and treatment which avoid mental suffering

The animal welfare assessment protocol for pigs, Welfare Quality® (WELFARE QUALITY®, 2009), states that good health, one of the principles of the animal welfare, is composed of three criteria: absence of injury, absence of disease and absence of pain induced by manager (Table 2). It is proposed to evaluate the first criterion on sows by verifying the presence of lameness. This is done visually, rating the animals in three levels: level 0 (normal gait, or the animal with difficulty on walking, but still using all four legs), level 1 (sow severely lame with asymmetric walking) and level 2 (animal cannot support any weight on affected limb, or cannot walk).

The good feeding, another principle proposed by the Welfare Quality®, is composed of two criteria: absence of prolonged hunger and absence of prolonged thirst. The first criterion must be assessed, in sows, by measuring the body condition of the animals. This is done visually and by touch, classifying the body condition in three levels: level 0 (sow in good condition, with well-developed muscles on the bone), level 1 (thin sow, with bones easily felt; or sow visually obese) and 2 (very thin sow, with the hips and backbone prominent).

For the quantification of these two principles, both the detection of lameness and the classification of body condition are done by subjective methods, dependent on the opinion of the handler, which can generate differences between ratings given by different people. Lameness causes pain and difficulty of locomotion (Anil, Anil, & Deen, 2009) and, however, it is a common disorder in sows that causes negative impacts on both welfare and production, since the animals that demonstrate this problem, have a smaller number of born-alive piglets, fewer gestations per year and are removed from the herd at a younger age than the ideal (Anil et al., 2009).

It is known that, during pregnancy, each sow should receive a different amount of food according to its body condition. Underweight animals present nutritional deficiency, fewer piglets born per litter, and those that are born, can present also nutritional deficiencies and smaller body mass (Eissen, Kanis, & Kemp, 2000). Overweight sows are usually larger than the space provided in the pen, which leads to stress for the animal and may cause death of piglets by crushing. In addition, overweight sows have an abnormal development of mammary glands, reducing

the amount of milk produced during lactation. Sows that are obese during pregnancy tend to reduce the amount of food ingested during lactation, which also reduces the amount of milk produced (Eissen et al., 2000).

Table 2. Evaluation of sows Welfare. Adapted from Welfare Quality® (2009).

Welfare Principles		Welfare Criteria	Measurements
Good feeding	1	Absence of prolonged hunger	Body condition score
	2	Absence of prolonged thirst	Water supply
Good housing	3	Comfort around resting	Bursitis, shoulder sores, absence of manure on the body
	4	Thermal comfort	Painting, huddling
	5	Ease of movement	Space allowance, farrowing crates
Good Health	6	Absence of injuries	Lameness, wounds on the body, vulva lesions
	7	Absence of disease	Mortality, coughing, sneezing, pumping, rectal prolapse, scouring, constipation, metritis, mastitis, uterine prolapse, skin condition, ruptures and hernias, local infections
	8	Absence of pain induced by management procedures	Nose ringing and tail docking
Appropriate behavior	9	Expression of social behaviors	Social behavior
	10	Expression of other behaviors	Stereotypies, exploratory behavior
	11	Good human-animal relationship	Fear of humans
	12	Positive emotional state	Qualitative Behavior Assessment (QBA)

Therefore, the early recognition of animals that present physical condition outside the ideal condition is important to prevent production losses caused by both the aggravation of the conditions presented and the impact on the animals' welfare. Some authors have been using ratings like those proposed by the Welfare Quality® to assess body condition of sows over the years (Charette, Bigras-Poulin, & Martineau, 1996; Esbenshade, Britt, Armstrong, Toelle, & Stanislaw, 1986; M. T. Knauer & Baitinger, 2015; Mark Knauer, Stalder, Baas, Johnson, & Karriker, 2012; Maes, Janssens, Delputte, Lammertyn, & De Kruif, 2004; Salak-Johnson, Niekamp, Rodriguez-Zas, Ellis, & Curtis, 2007) (Patience & Thacker, 1989). In most of the cases, this classification is done using a scale from 1 to 5, ranging from very thin to obese. The classification proposed by Patience & Thacker (1989) is the most used and estimates the fat reserves of the animal through both visual assessment and the pressing of the pelvic girdle of the animal, using the fingers (Table 3).
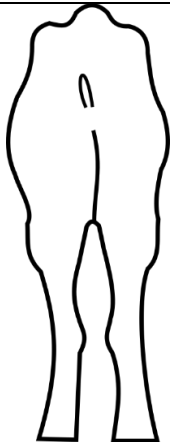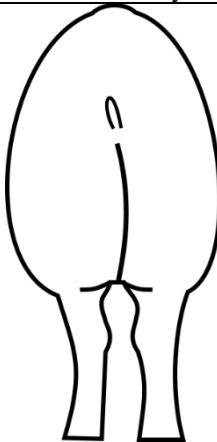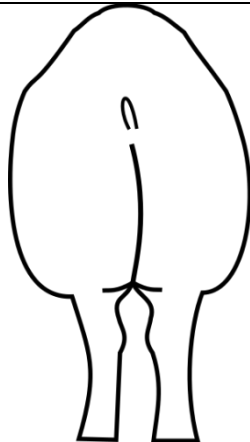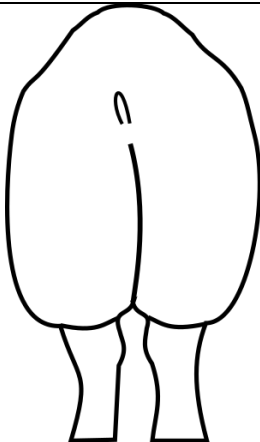
The most common method to quantify lameness is also the visual score. The scoring systems proposed by Main, Clegg, Spatz, & Green (2000) and by the Welfare Quality® are the most used. That method consists in classifying the gait of the animals on a scale from 0 to 5, ranging from an animal that shows no lameness (score of 0) to an animal that can't stand up (score of 5).

As alternatives to these subjective methods of classification, various methods have been proposed to obtain a more objective measure. For lameness, kinetics and kinematics have been widely used in horses and cows and they began to be used in pigs. The kinetics aims to relate the movement of the bodies with their causes and considers the dynamic forces and acceleration. The footprint was analyzed in many species to study locomotion disorders. One of the possibilities of kinetic is to study simultaneously the positioning of the four legs and quantify parameters that cannot be measured with kinematics, such as slips when walking, trodden angles and the area of limbs in contact with the floor (Nalon, Conte, Maes, Tuyttens, & Devillers, 2013). The use of a hallway with floor covered in clay has been tested for acquiring the footprints of sows (Grégoire, Bergeron, D'Allaire, Meunier-Salaün,

& Devillers, 2013), but it has not been possible to establish a relationship between the footprint pattern and the level of lameness, perhaps because of the floor type used.

Kinematic analysis quantifies the characteristics of the animal's gait in the form of measures related with time, distance and angles that describe the movements of the body segments and the joint angles. This analysis is made using reflective markers in predetermined locations on the body of the animal and video recording of the gait. With this technique, several parameters can be analyzed simultaneously by an auto-tracking software, however, some problems have been associated with it, mainly related with the placing of markers and their movement with the walk, the difficulty in finding joints or bones located behind muscle and fat where these markers will be positioned, and repeatability of positioning (Nalon et al., 2013). Despite the problems, this method has been effective showing (Grégoire et al., 2013) that lame sows have lower walking speed, spend less time standing during a period of 24 hours and tend to step more often during the time following the feeding.

Table 3. Body condition score of sows. Adapted from Patience & Thacker (1986).

Body condition Score				
1	2	3	4	5
Too thin	Skinny	Ideal	Overweight	Obese
Prominent hip bones and spine	Hip bones and spine easily felt without applying pressure.	Hip bones and spine felt only with palm pressure application.	Hip bones and spine cannot be felt.	Hip bones and spine thickly covered with fat.

At the end of the 90's, it was noted (Charette et al., 1996) the need for evaluation of body condition of sows using not just subjective methods of classification, but also more objective values, as body mass, the thickness of subcutaneous fat and dimensions of the animal, taking into consideration the parity of the animals. This type of classification, covering a larger number of variables, was adopted more recently (Sell-Kubiak, 2015) and expanded, using also the duration of the sow's gestation as a factor to be considered, proposing a classification of the sow's body condition throughout gestation and lactation, and obtaining measures of body mass and backfat thickness at the time of insemination, after birth and after weaning.

To reduce the errors with the body condition scoring, one should try to reduce the variation generated by the classification done by different managers. A way of doing that was proposed by Knauer & Baitinger, 2015, who developed a caliper that quantifies the angularity from the spinous process to the transverse process of a sow's back and concluded that this instrument can be used as a tool to standardize this classification.

Another way to standardize this measurement would be to automate the process by analyzing images generated by depth cameras. This method has already been used for dairy cows (Kuzuhara et al., 2015), obtaining a correlation of 74% between the predicted and actual body condition score. This can indicate the possibility of using this method for sows. In addition to the body condition classification by scores, one can also combine it with data of backfat thickness, body mass, parity and dimensions of sows to obtain a new classification regarding the body condition of these animals as soon as these parameters have been proved to be effective in the body characterization of sows (Charette et al., 1996; Sell-Kubiak, 2015).

The most used method for acquiring the backfat thickness (De Rensis, Gherpelli, Superchi, & Kirkwood, 2005; Kim et al., 2016; M. T. Knauer & Baitinger, 2015; Maes et al., 2004; Magowan & McCann, 2006) is obtaining it through ultrasonic probes. One problem with this approach is the difficulty of applying it on an industrial scale, since this assessment should be manually done for each animal. Noticing this difficulty in the production of dairy cows, Weber et al., 2014 proposed the use of a depth camera for prediction of the animals' backfat, obtaining a correlation of 96% with the fat thickness measured with ultrasonic probes. This indicates the possibility of using this method on sows to predict their backfat.

Weighing is a time consuming and stressful practice for both the animal and the handler. Taking this into account, several authors (Frost et al., 1997; Kashiha et al., 2014; Kongsro, 2014; Schofield, 1990; Schofield, 1999; Wu et al., 2004) have been using pigs' dimensions data for predicting animal's mass. To replace the scale by an indirect method, both the convenience and the accuracy of the method to be used should be considered. Different methods of obtaining pigs' mass have been tested by many authors (Philips & Dawson, 1936; Zagaroza, 2009). The use of calipers and tape is shown to be effective to this end, but the need to restrict the animals to obtain the data, makes this process impracticable on an industrial scale and equivalent to the process of weighing itself. With that, the use of images to obtain pigs' dimensions would be interesting because of its non-invasive approach.

The potential of using images for calculating dimensions was noted by other authors (Kashiha et al., 2014; Schofield, 1990; Schofield, 1999; Wang, Yang, Winter, & Walker, 2008; Wu et al., 2004), which correlated the animals' area obtained through images with their mass and developed prediction equations. In general, these authors point to the fact that to extract the pigs' dimensions, their skin and hair colors must be distinct from the environment color. Dark, stained or dirty animals hinder the automation of this approach. In addition to the color of the animal, the presence of adequate light is critical for this application. Kashiha et al. (2014) found great lighting values within the range of 40 to 150 lux. To avoid this problem, it was developed (Wu et al., 2004) an image capture system with six high-resolution cameras (3032 × 2028 pixels) and three flash units to obtain the 3-D forms of live pigs. However, the excess equipment and the high costs involved make it difficult to use this type of image capturing on an industrial scale.

A different approach has been used (I.C.F.S. Condotta, Brown-Brandl, Silva-Miranda, & Stinn, 2018; Kongsro, 2014; Pezzuolo, Guarino, Sartori, González, & Marinello, 2018), applying depth cameras to obtain pigs' mass (grow-finish pigs). This information is obtained from the correlation between the body volume generated from the depth images and the mass of the animal. This approach reduces concerns about calibration and lighting, in addition to providing the animal's height.

These depth cameras have been used in many areas, such as 3D mapping and reconstruction (Izadi et al., 2011, Jia et al., 2012), indoor robotics (Correa et al., 2012; Ganganath & Leung, 2012; Benavidez & Jamshidi, 2011), object detection and recognition (Hernández-López et al., 2012) and recognition of gestures (Chang et al., 2011 (a); Chang et al., 2011 (b), Hondori et al., 2012). A commercial sensor that is being used (I.C.F.S. Condotta et al., 2018;

Kongsro, 2014; Kulikov et al., 2014; Lao et al., 2016; Lee, Kim, Lim, & Ahn, 2016; Pezzuolo et al., 2018; Stavrakakis et al., 2015; Zhu, Ren, Barclay, McCormack, & Thomson, 2015), as an alternative to expensive laser scanners (Khoshelham & Elberink, 2012) and stands out for its low cost, reliability and measurement speed (Smisek et al., 2015) is the Microsoft Kinect sensor. The version 1 (Figure 1) of this sensor uses structured light technology, which is the process of projecting a known pattern into a scene or object and obtaining depth values according to its reflection pattern. For that, the emitter projects a beam of light in the near infrared region and the infrared camera is triggered to obtain the infrared image, which contains the pattern of dots of reflected light in the scene. Another commercial sensor that also uses the structured light technology and is being applied (H. Guo et al., 2017; Y. Guo, Zhu, Jiao, & Chen, 2014; Kuzuhara et al., 2015) in the animal area is the Xtion® Pro, from Asus (Figure 2).
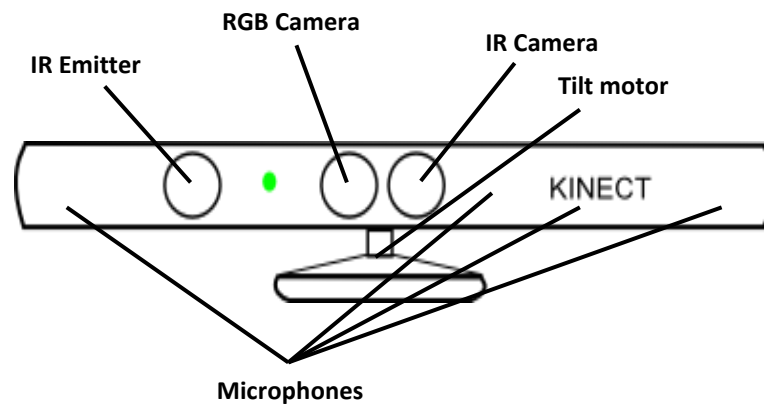
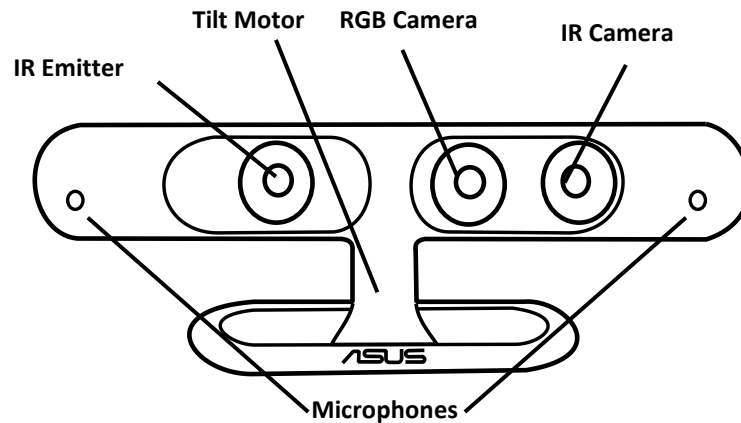**Figure 1.** Microsoft Kinect sensor v.1 components.

Figure 2. Asus Xtion® Pro sensor components.

14

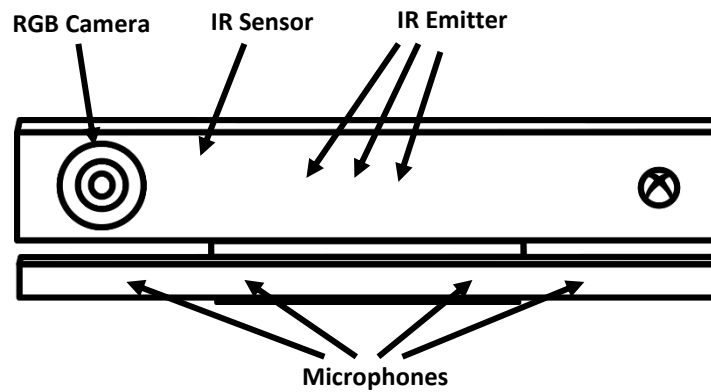**RGB Camera**   **IR Sensor**   **IR Emitter**

Microphones

Figure 3. Microsoft Kinect sensor v.2 components.

According to the technical specifications provided by Microsoft, the version 2 of the Kinect sensor (Figure 3) is composed by an RGB camera, three infrared (IR) emitters, an infrared depth sensor and four multi-array microphones, and presents less problems with capturing images in widely lit environments when compared to the first version of the sensor. Three image outputs are provided by Kinect: (1) RGB image with 1920 x 1080 pixels, (2) IR image with 512 x 424 pixels, and (3) depth image with 512 x 424 pixels, in addition to the possibility of audio capture. Parallel to the depth image, a numerical map is generated, which is the main raw data provided by the sensor, containing the distances, in mm, between the sensor and each pixel that makes up the image. For generating the depth image, this second version of the sensor uses the time-of-flight technology, which is based on the principle that, "knowing the speed of light, the distance to be measured is proportional to the time required by the active lighting source to travel from the emitter to the target"(Lachat, Macher, Mittet, Landes, & Grussenmeyer, 2015).

The present work aimed to obtain three characteristics (body condition score, body mass and backfat thickness) of sows using a commercially available depth camera, that proved to be effective in obtaining these characteristics in other animals (dairy cows). In addition, with the same sensor, a method for early detection of lameness in sows was developed, using the kinematic of animal's approach, that has been giving good results and which difficulties have the potential to be overcame using a depth camera instead of the method of reflective markers currently used.

References

Anil, S. S., Anil, L., & Deen, J. (2009). Javma.235.6.734 (1). 235(6).

Benavidez, P., & Jamshidi, M. (2011, June). Mobile robot navigation and target tracking system. In 2011 6th International Conference on System of Systems Engineering (pp. 299-304). IEEE.

Charette, R., Bigras-Poulin, M., & Martineau, G. P. (1996). Body condition evaluation in sows. Livestock Production Science, 46(2), 107–115. https://doi.org/10.1016/0301-6226(96)00022-X

Chang, Y. J., Chen, S. F., & Chuang, A. F. (2011). A gesture recognition system to transition autonomously through vocational tasks for individuals with cognitive impairments. Research in developmental disabilities, 32(6), 2064-2068.

Chang, Y. J., Chen, S. F., & Huang, J. D. (2011). A Kinect-based system for physical rehabilitation: A pilot study for young adults with motor disabilities. Research in developmental disabilities, 32(6), 2566-2570.

Condotta, I. C. F. S., Brown-Brandl, T. M., Silva-Miranda, K. O., & Stinn, J. P. (2018). Evaluation of a depth sensor for mass estimation of growing and finishing pigs. Biosystems Engineering, 173. https://doi.org/10.1016/j.biosystemseng.2018.03.002

Correa, D. S. O., Sciotti, D. F., Prado, M. G., Sales, D. O., Wolf, D. F., & Osorio, F. S. (2012, May). Mobile robots navigation in indoor environments using Kinect sensor. In 2012 Second Brazilian Conference on Critical Embedded Systems (pp. 36-41). IEEE.

De Rensis, F., Gherpelli, M., Superchi, P., & Kirkwood, R. N. (2005). Relationships between backfat depth and plasma leptin during lactation and sow reproductive performance after weaning. Animal Reproduction Science, 90(1–2), 95–100. https://doi.org/10.1016/j.anireprosci.2005.01.017

Eissen, J. J., Kanis, E., & Kemp, B. (2000). Sow factors affecting voluntary feed intake during lactation. Livestock Production Science, 64(2–3), 147–165. https://doi.org/10.1016/S0301-6226(99)00153-0

Esbenshade, K. L., Britt, J. H., Armstrong, J. D., Toelle, V. D., & Stanislaw, C. M. (1986). Body condition of sows across parities and relationship to reproductive performance. Journal of Animal Science, 62(5), 1187–1193. https://doi.org/10.2527/jas1986.6251187x

Frost, A. R., Schofield, C. P., Beaulah, S. A., Mottram, T. T., Lines, J. A., & Wathes, C. M. (1997). A review of livestock monitoring and the need for integrated systems. Computers and electronics in agriculture, 17(2), 139-159.

Ganganath, N., & Leung, H. (2012, January). Mobile robot localization using odometry and kinect sensor. In 2012 IEEE International Conference on Emerging Signal Processing Applications (pp. 91-94). IEEE.

Grégoire, J., Bergeron, R., D'Allaire, S., Meunier-Salaün, M.-C., & Devillers, N. (2013). Assessment of lameness in sows using gait, footprints, postural behaviour and foot lesion analysis. Animal, 7(07), 1163–1173. https://doi.org/10.1017/s1751731113000098

Guo, H., Ma, X., Ma, Q., Wang, K., Su, W., & Zhu, D. H. (2017). LSSA_CAU: An interactive 3d point clouds analysis software for body measurement of livestock with similar forms of cows or pigs. Computers and Electronics in Agriculture, 138, 60–68. https://doi.org/10.1016/j.compag.2017.04.014

Guo, Y., Zhu, W., Jiao, P., & Chen, J. (2014). Foreground detection of group-housed pigs based on the combination of Mixture of Gaussians using prediction mechanism and threshold segmentation. Biosystems Engineering, 125, 98–104. https://doi.org/10.1016/j.biosystemseng.2014.07.002

Hernandez-Lopez, J. J., Quintanilla-Olvera, A. L., López-Ramírez, J. L., Rangel-Butanda, F. J., Ibarra-Manzano, M. A., & Almanza-Ojeda, D. L. (2012). Detecting objects using color and depth segmentation with Kinect sensor. Procedia Technology, 3, 196-204.

Hondori, H. M., Khademi, M., & Lopes, C. V. (2012, November). Monitoring intake gestures using sensor fusion (microsoft kinect and inertial sensors) for smart home tele-rehab setting. In 2012 1st Annual IEEE Healthcare Innovation Conference.

Izadi, S., Kim, D., Hilliges, O., Molyneaux, D., Newcombe, R., Kohli, P., ... & Fitzgibbon, A. (2011, October). KinectFusion: real-time 3D reconstruction and interaction using a moving depth camera. In Proceedings of the 24th annual ACM symposium on User interface software and technology (pp. 559-568). ACM.

Jia, W., Yi, W. J., Saniie, J., & Oruklu, E. (2012, May). 3D image reconstruction and human body tracking using stereo vision and Kinect technology. In 2012 IEEE International Conference on Electro/Information Technology (pp. 1-4). IEEE.

Kashiha, M., Bahr, C., Ott, S., Moons, C. P. H., Niewold, T. A., Ödberg, F. O., & Berckmans, D. (2014). Automatic weight estimation of individual pigs using image analysis. Computers and Electronics in Agriculture, 107, 38–44. https://doi.org/10.1016/j.compag.2014.06.003

Khoshelham, K., & Elberink, S. O. (2012). Accuracy and resolution of kinect depth data for indoor mapping applications. Sensors, 12(2), 1437-1454.

Kim, K. H., Hosseindoust, A., Ingale, S. L., Lee, S. H., Noh, H. S., Choi, Y. H., … Chae, B. J. (2016). Effects of gestational housing on reproductive performance and behavior of sows with different backfat thickness. Asian-Australasian Journal of Animal Sciences, 29(1), 142–148. https://doi.org/10.5713/ajas.14.0973

Knauer, M., Stalder, K., Baas, T., Johnson, C., & Karriker, L. (2012). Physical Conditions of Cull Sows Associated with On-Farm Production Records. Open Journal of Veterinary Medicine, 02(03), 137–150. https://doi.org/10.4236/ojvm.2012.23023

Knauer, M. T., & Baitinger, D. J. (2015). The sow body condition caliper. Applied Engineering in Agriculture, 31(2), 175–178. https://doi.org/10.13031/aea.31.10632

Kongsro, J. (2014). Estimation of pig weight using a Microsoft Kinect prototype imaging system. Computers and Electronics in Agriculture, 109, 32–35. https://doi.org/10.1016/j.compag.2014.08.008

Kulikov, V. A., Khotskin, N. V., Nikitin, S. V., Lankin, V. S., Kulikov, A. V., & Trapezov, O. V. (2014). Application of 3-D imaging sensor for tracking minipigs in the open field test. Journal of Neuroscience Methods, 235, 219–225. https://doi.org/10.1016/j.jneumeth.2014.07.012

Kuzuhara, Y., Kawamura, K., Yoshitoshi, R., Tamaki, T., Sugai, S., Ikegami, M., … Yasuda, T. (2015). A preliminarily study for predicting body weight and milk properties in lactating Holstein cows using a three-dimensional camera system. Computers and Electronics in Agriculture, 111, 186–193. https://doi.org/10.1016/j.compag.2014.12.020

Lachat, E., Macher, H., Mittet, M. A., Landes, T., & Grussenmeyer, P. (2015). First experiences with kinect V2 sensor for close range 3D modelling. International Archives of the Photogrammetry, Remote Sensing and Spatial Information Sciences - ISPRS Archives, 40(5W4), 93–100. https://doi.org/10.5194/isprsarchives-XL-5-W4-93-2015

Lao, F., Brown-Brandl, T., Stinn, J. P., Liu, K., Teng, G., & Xin, H. (2016). Automatic recognition of lactating sow behaviors through depth image processing. Computers and Electronics in Agriculture, 125, 56–62. https://doi.org/10.1016/j.compag.2016.04.026

Lee, S., Kim, J., Lim, H., & Ahn, S. C. (2016). Surface reflectance estimation and segmentation from single depth image of ToF camera. Signal Processing: Image Communication, 47, 452–462. https://doi.org/10.1016/j.image.2016.07.006

Maes, D. G. D., Janssens, G. P. J., Delputte, P., Lammertyn, A., & De Kruif, A. (2004). Back fat measurements in sows from three commercial pig herds: Relationship with reproductive efficiency and correlation with visual body condition scores. Livestock Production Science, 91(1–2), 57–67. https://doi.org/10.1016/j.livprodsci.2004.06.015

Magowan, E., & McCann, M. E. E. (2006). A comparison of pig backfat measurements using ultrasonic and optical instruments. Livestock Science, 103(1–2), 116–123. https://doi.org/10.1016/j.livsci.2006.02.002

Main, D. C. J., Clegg, J., Spatz, A., & Green, L. E. (2000). Repeatability of a lameness scoring system for finishing pigs. Veterinary Record, 147(20), 574–576. https://doi.org/10.1136/vr.147.20.574

Nalon, E., Conte, S., Maes, D., Tuyttens, F. A. M., & Devillers, N. (2013). Assessment of lameness and claw lesions in sows. Livestock Science, 156(1–3), 10–23. https://doi.org/10.1016/j.livsci.2013.06.003

Patience, J. F., & Thacker, P. A. (1989). Swine nutrition guide (No. 636.4 P2737s Ej. 1 009811). University of Saskatchewan.

Pezzuolo, A., Guarino, M., Sartori, L., González, L. A., & Marinello, F. (2018). On-barn pig weight estimation based on body measurements by a Kinect v1 depth camera. Computers and Electronics in Agriculture, 148(August 2017), 29–36. https://doi.org/10.1016/j.compag.2018.03.003

Phillips, R. W., & Dawson, W. M. (1936). A study of methods for obtaining measurements of swine. Journal of Animal Science, 1936(1), 93-99.

Salak-Johnson, J. L., Niekamp, S. R., Rodriguez-Zas, S. L., Ellis, M., & Curtis, S. E. (2007). Space allowance for dry, pregnant sows in pens: Body condition, skin lesions, and performance. Journal of Animal Science, 85(7), 1758–1769. https://doi.org/10.2527/jas.2006-510

Schofield, C. P. (1990). Evaluation of image analysis as a means of estimating the weight of pigs. Journal of Agricultural Engineering Research, 47(C), 287–296. https://doi.org/10.1016/0021-8634(90)80048-Y

Schofield, C. P., Marchant, J. A., White, R. P., Brandl, N., & Wilson, M. (1999). Monitoring pig growth using a prototype imaging system. Journal of Agricultural Engineering Research, 72(3), 205-210.

Sell-Kubiak, E. (2015). Non-genetic variance in pigs: genetic analysis of production and reproduction traits.

Smisek, J., Jancosek, M., & Pajdla, T. (2013). 3D with Kinect. In Consumer depth cameras for computer vision (pp. 3-25). Springer, London.

Stavrakakis, S., Li, W., Guy, J. H., Morgan, G., Ushaw, G., Johnson, G. R., & Edwards, S. A. (2015). Validity of the Microsoft Kinect sensor for assessment of normal walking patterns in pigs. Computers and Electronics in Agriculture, 117, 1–7. https://doi.org/10.1016/j.compag.2015.07.003

Wang, Y., Yang, W., Winter, P., & Walker, L. (2008). Walk-through weighing of pigs using machine vision and an artificial neural network. Biosystems Engineering, 100(1), 117–125. https://doi.org/10.1016/j.biosystemseng.2007.08.008

Weber, A., Salau, J., Haas, J. H., Junge, W., Bauer, U., Harms, J., … Thaller, G. (2014). Estimation of backfat thickness using extracted traits from an automatic 3D optical system in lactating Holstein-Friesian cows. Livestock Science, 165(1), 129–137. https://doi.org/10.1016/j.livsci.2014.03.022

WELFARE QUALITY®. Welfare Quality® assessment protocol for pigs (sows and piglets, growing and finishing pigs). Lelystad, Netherlands: Welfare Quality® Consortium, 2009. 123 p.

Wu, J., Tillett, R., McFarlane, N., Ju, X., Siebert, J. P., & Schofield, P. (2004). Extracting the three-dimensional shape of live pigs using stereo photogrammetry. Computers and Electronics in Agriculture, 44(3), 203–222. https://doi.org/10.1016/j.compag.2004.05.003

Zaragoza, L. E. O. (2009). Evaluation of the accuracy of simple body measurements for live weight prediction in growing-finishing pigs. MSc. Diss. Univ. of Illinois, Urbana, Illinois.

Zhu, Q., Ren, J., Barclay, D., McCormack, S., & Thomson, W. (2015). Automatic animal detection from Kinect sensed images for livestock monitoring and assessment. Proceedings - 15th IEEE International Conference on Computer and Information Technology, CIT 2015, 14th IEEE International Conference on Ubiquitous Computing and Communications, IUCC 2015, 13th IEEE International Conference on Dependable, Autonomic and Se, 1154–1157. https://doi.org/10.1109/CIT/IUCC/DASC/PICOM.2015.172

2   MAIN RESULTS AND DISCUSSION

This thesis was divided into three papers that will be sent for publication this year. The first paper will be sent for publication on the Computers and Electronics in Agriculture journal and covers a study of the current available depth sensing technologies and evaluate its use on precision animal management applications. The second and third papers will be both send for publication on the Biosystems Engineering journal. The second paper covers the body condition characterization of sows through depth images, and the third paper covers the detection of lameness on sows also through depth images.

On the first paper unit transformation equations were developed. These equations make it possible to determine the actual dimensions of an object (length, area and volume), in metric units, from its dimensions in the image, in pixels, based on the distance between the object and the sensor, that can be easily obtained with depth cameras. These equations are an advantage on animal applications that use computer vison because they eliminate the need for the presence of an object with pre-determined dimensions on the image. This facilitate the images analysis and the automation of the process.

These equations developed were used on the third chapter of this thesis to obtain dimensions of animals in metric units. Also, one of the conclusions of this first paper was that the time-of-flight technology is the best to be used for indoor applications and the combination of stereo vision with structured light is the best for outdoor applications. With that in mind, Kinect v.2 camera was selected to be used on both the second and third papers, as it is a low-cost depth camera that uses the time-of-flight technology.

On the second paper, body condition, backfat and weight were assessed using a depth camera. For that, a multiple linear regression was obtained using the minor axis of the ellipse fitted around sow's body, the width at shoulders, and the angle, of the last rib's curvature to predict body condition. To predict backfat, a multiple linear regression was performed using the height of last rib's curvature, the perimeter of sow's body, the major axis of the ellipse fitted around sow's body, the length from snout to rump, and the predicted body condition score. It was possible to obtain the body mass with a simple linear regression using the projected volume of the sows' body.

As for the third paper, lameness was assessed on sows using one of the three models: linear discriminant analysis, fine 1-nearest neighbor, and weighted 10-nearest neighbors; and input variables obtained from depth videos (number, time, and length of steps for each of the four regions analyzed - left and right shoulders and left and right hips; total walk time; and number of local maxima for head region).

For both papers that assessed the physical conditions of sows, the errors obtained were in acceptable levels (7.7% for body condition scoring, 16.1% for backfat, 3.8% for weight, and 33.1% for lameness classification) when compared with the literature. These works indicate that automation through image processing could be possible. The next steps would be to try to reduce the errors found. One problem with this is the difficulty in correctly identifying subjectively score data as a standard to be used as a comparison. An alternative would be to develop a completely new physical condition classification system based on image processing, that would take into consideration the way that dimensions and behavior of individual animals change over time, rather than try to predict the current indicators of good physical condition (e.g. body condition score, backfat, weight , and lameness presence). This could aid producers to take better and faster management decisions, with a reduced stress level for both workers and animals, improving animal well-being and maximizing the profitability of swine production.

3 EVALUATION OF LOW-COST DEPTH CAMERAS FOR PRECISION LIVESTOCK FARMING APPLICATIONS

Abstract

Low-cost depth-cameras have been used in many agricultural applications. These cameras use one or a more of these three technologies: structured light (SL), time-of-flight (ToF), and stereovision (SV). The objectives were to 1) evaluate different technologies for depth sensing, including measuring, accuracy, and repeatability of distance data, and 2) to compare these parameters at different positions within the image, and 3) determine each camera's usefulness in indoor and outdoor settings. Then, cameras were tested in a swine facility. Five different cameras were used: (1) Microsoft Kinect v.1 (SL), (2) Microsoft Kinect v.2 (ToF), (3) Intel® RealSense™ Depth Camera D435 (SL, SV), (4) ZED Stereo Camera (StereoLabs; SV), and (5) CamBoard Pico Flexx (PMD Technologies, ToF). Results indicate that there were significant differences for all cameras (P<0.05), except for ToF cameras (Kinect v.2 and Flexx). All cameras showed an increase in the standard deviation as the distance between camera and object increased; however, the Intel RealSense camera had a larger increase. Time-of-flight cameras had the smallest error between different sizes of objects. All cameras showed some distortion at the edges of the images, and ToF cameras had non-readable zones on the corners of the images. In conclusion, understanding the errors associated with each type of technology is important for capturing useful data. It was concluded that the ToF technology is the best to be used for indoor applications and the combination of SV with SL is the best for outdoor applications.

Keywords: Depth image, Time-of-flight, Stereo vision, Structured light

3.1 Introduction

Low-cost depth cameras have been used as an alternative to expensive laser scanners (Khoshelham & Elberink, 2012) in various areas, such as mapping and 3D reconstruction (Izadi, Kim, & Hilliges, 2011), indoor robotics (Benavidez, 2011; Correa et al., 2012; Ganganath & Leung, 2012), objects' detection and recognition (Hernández-López et al., 2012), and gesture recognition (Chang, Chen, & Huang, 2011; Chang, Wang, & Chen, 2011). Most of these areas were originally approached using standard digital image processing and analyzing, but problems with this approach, such as lighting, color distinction and excess of equipment, led to the use of depth cameras.

There are several technologies used for depth acquisition. Stereo vision was the first one used to acquire information on the objects' geometry. The structured light (SL) technology was introduced to overcome some of the problems with the stereovision and, after that, the time-of flight cameras started being used.

Depth images provided by these cameras are composed of a numeric map containing the distances, most commonly in metric units, between the sensor and each pixel that makes up the image. Depth cameras have been used in a variety of agricultural applications (Condotta et al., 2018; Guo et al., 2017; Hao & Shengli, 2014; Kongsro, 2014; Kulikov et al., 2014; Lao et al., 2016; Lee, Jin, Park, & Chung, 2016; Stavrakakis et al., 2015; Wang et al., 2018; Zhu, Ren, Barclay, McCormack, & Thomson, 2015). The advantages that have been noted include low cost, reliability and speed of measurement. However, some problems that have been noted are occlusion, (difficulty of acquiring reliable data on environments with excess of light, preventing its use for outdoors applications), shape distortion; motion blur, and noise. These issues are related to the technology used. Understanding the limitations of each type of depth camera technology will provide a basis for the technology selection and the development of research involving its use.

Khoshelham & Elberink (2012) examined the accuracy and precision of the depth data provided by a Kinect sensor v.1 and provided an explanation of various errors. The random error of measurements fluctuated

between a few millimeters to 4 cm; this error tended to increase with distance between sensor and object and. In addition, the errors in the distance data originated from three sources: (1) calibration errors, (2) configuration of the measuring area (improper lighting, or image geometry), and (3) smooth or bright surfaces. While lighting is generally not a problem with these depth cameras for indoor applications, intense lighting can generate low contrast in the infrared image and, therefore, result in gaps on the depth image. These gaps can also occur when the distance from the object to the sensor is outside of the operating range, or when the orientation of the object surface is such that the emitter does not illuminate some areas, or the camera fails to capture information. Surfaces that are too bright or smooth are very reflective and can also prevent measurement.

Generally, depth cameras' error is low (Dutta, 2012); however, the standard deviation of the distance data increases with increasing distance between sensor and object and is greater on the corners of the image. In addition, depth data has been reported to be unusable or inaccurate on the object edges because, in these areas, the depth map is obtained through interpolation of the projections of the reflected infrared light on two different regions, the edge and the background (Gottfried, Fehr, & Garbe, 2011). For studies capturing specific distance data that use more than one depth camera there is a need to know the relative differences between the cameras and its captured data.

3.1.1 Technologies' principles

There is a variety of commercial depth cameras that have being used on agricultural applications (Table 1). Currently, Kinect (v.1 and v.2) and Xtion PRO Live are not available on market. Technology used by these depth cameras can be divided into 3 different principles: stereovision (SV), structured light (SL), and Time-of-flight (ToF). To form the depth image, SV cameras use two RGB cameras to acquire images from the same scene at slightly different positions. The 3-dimensional position of a point on the scene is calculated by triangulation between corresponding points on both images(Berkovic & Shafir, 2012; Keselman, Woodfill, Grunnet-Jepsen, & Bhowmik, 2017). Structured light cameras form the depth image by using the IR emitter to project a beam of light that is divided into multiple beams when reflected on the objects, forming a pattern of points which are captured by the IR camera. This pattern is compared with a standard of predetermined distance from the camera. The distance from each pixel to the camera is calculated by triangulation (Andersen et al., 2012; Berkovic & Shafir, 2012; Sarbolandi, Lefloch, & Kolb, 2015; Zhang, 2018). The time-of-flight (ToF) cameras use a technology that is based on measuring the time that the light emitted by the IR emitter requires to travel to a scene and back to the camera. The IR light is then captured by the IR camera, and, using speed of light, it is possible to calculate the distance traveled (Sarbolandi et al., 2015).

Table 1. Comparison of commercial depth cameras.

Camera	Principle	Measuring Range (m)	Depth Resolution	RGB Max Resolution	Frame Rate (FPS)	FoV (HxV)	Price (US$)
Kinect v.1	SL	0.4 – 3.5	640 x 480	640 x 480	15/30	57° x 43°	250
Xtion PRO	SL	0.8 – 3.5	640 x 480	1280 x 1024	30/60	58° x 45°	140
Xtion 2	SL	0.8 – 3.5	640 x 480	2592 x 1944	30	74° x 52°	236
Kinect v.2	ToF	0.5 – 4.5	512 x 424	1920 x 1080	15/30	70° x 60°	140
Pico Flexx	ToF	0.1 – 4.0	224 x 171	-	45	62° x 45°	390
Pico Monstar	ToF	0.5 – 6.0	352 x 287	-	60	100° x 85°	1930
ZED	SV	0.5 - 20	2208 x 621	2208 x 621	15/30/60/100	90° x 60°	450
RealSense D415	SL+SV	0.16 – 10	1280 x 720	1920 x 1080	90	63° x 40°	150
RealSense D435	SL+SV	0.11 - 10	1280 x 720	1920 x 1080	90	85° x 58°	180

3.1.2 Objectives

The objective of this study was to evaluate different technologies for depth sensing, including (1) measure the accuracy and repeatability of distance data, (2) measure the accuracy and repeatability of dimensions data relative to positions within the image and distance from the camera, (3) develop unit transformation equations for each camera, (4) determine the maximum useful distance and the associated errors for each camera in indoor and outdoor settings, (5) test each camera to evaluate its usefulness in collecting phenotypic data of livestock.

3.2 Materials and Methods

The work was composed of four experiments. For all experiments, five different types of cameras were used: (1) Microsoft Kinect v.1 (Figure 1a), (2) Microsoft Kinect v.2 (Figure 1b), (3) Intel® RealSense™ Depth Camera D435 (Figure 1c), (4) ZED Stereo Camera (StereoLabs) (Fig. 1d), and (5) CamBoard Pico Flexx (PMD Technologies) (Figure 1e). These cameras represent different technologies currently being used on agricultural research (ToF, SV combined with SL, SL, ToF and SV, respectively). Because Microsoft Kinect v.2 has being discontinued and, at the same time, is one of the most used depth cameras in agricultural research, another low-cost ToF camera was tested along with this camera.

Two types of programs were developed: (1) image acquisition programs and (2) image processing programs. For image acquisition, different programing environments were used for each camera. For CamBoard Pico Flexx and the Kinect cameras v.1 and v.2, a numerical computing software (MATLAB, R2018a) on a Windows computer was used. For Intel® RealSense™ camera, a C++ program was developed on an UP-Core board with an Ubuntu kernel using Intel® RealSense™ SDK, and, for ZED camera, a C++ program was developed on a NVIDIA Jetson TX2 board, also with an Ubuntu kernel, using ZED SDK. All the image processing programs were developed on a Windows computer using MATLAB, R2018a.
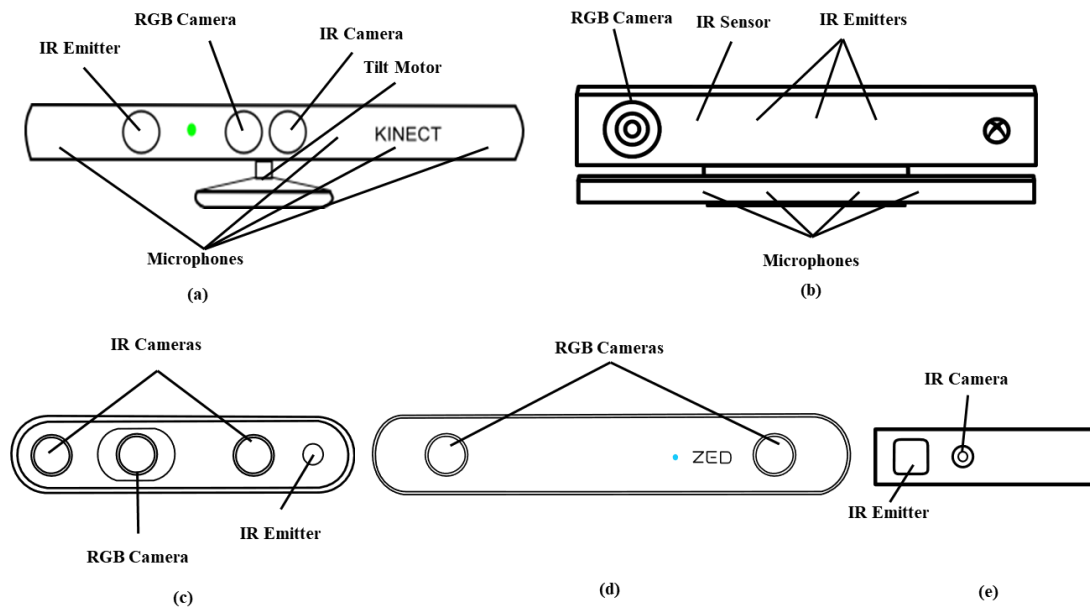
Figure 1. Components of commercial depth cameras being used in this study (out of scale). (a) Microsoft Kinect v.1, (b) Microsoft Kinect v.2, (c) Intel® RealSense™ Depth Camera D435, (d) ZED Stereo camera (StereoLabs) and (e) CamBoard Pico Flexx (PMD Technologies).

The livestock experiment was conducted in a grow-finish building at the USDA-ARS Meat Animal Research Center (USMARC) in Clay Center, Nebraska (-98.13° W, 42.52° N). Digital RGB color images, depth images, and masses were collected on a population of grow-finish pigs at three different time-points. All animal procedures were approved by the USMARC IACUC and followed recognized guidelines for animal use and care (FASS, 2010).

3.2.1 Distance accuracy and repeatability

A total of three depth cameras of each of the test types of cameras were compared for repeatability between sensors. Each camera was used to collect images of a wall at five distances (from 1.0 to 3.0 meters, every 0.5 m) (Figure 2). Five depth images and five RBG images (except for Pico Flexx) from each camera were collected.

Figure 2. Positioning of the components of the experiment: (a) table with depth cameras and computer for data acquisition and (b) markings on the floor (0.5 m from each other) to capture images of the wall at different distances (from 0.5m to 3.0 m).

Depth images were processed with an algorithm developed to extract a fixed area of 11 X 11 pixels at the center of the wall. These points were recorded and, then, the average and the standard deviation were calculated.

To evaluate the repeatability of the depth data provided by the cameras, a multiple linear regression model was developed in Excel® software, using dummy variables (Draper & Smith, 1998), which included the effects of all the cameras in the equation. This model was compared with a reduced model (simple linear regression) that did not include the individual effects of each camera.

This comparison was made by using the Efroymson's algorithm ("stepwise" regression) (Efroymson, 1960) for comparing two regression models, with null hypothesis given the reduced model equivalent to the global model and with alternative hypothesis, considering the models non-equivalent. The test statistic is given in eq. (1).

$$F(n, d) = \frac{(SS_r - SS_g)/(DF_r - DF_g)}{SS_g/DF_g} \tag{1}$$

where:

SS_r = sum of the squares of the residue of the reduced model;

SS_g = sum of the squares of the residue of the global model;

DF_r = degrees of freedom of the residue of the global model;

DF_g = degrees of freedom of the residue of the reduced model.

3.2.2 Dimension accuracy and repeatability

Three cameras of each type were used. Three sizes of poster board squares (10, 20, 30 cm²) were recorded at five distances (1.0 to 3.0 m; every 0.5 m) and four different positions on the image (center, edge on the horizontal axis, edge on the vertical axis, and corner; Figure 3). A total of five depth and RGB images (except CamBoard Pico Flexx) from each of the three replicates of the 5 types of cameras was collected.
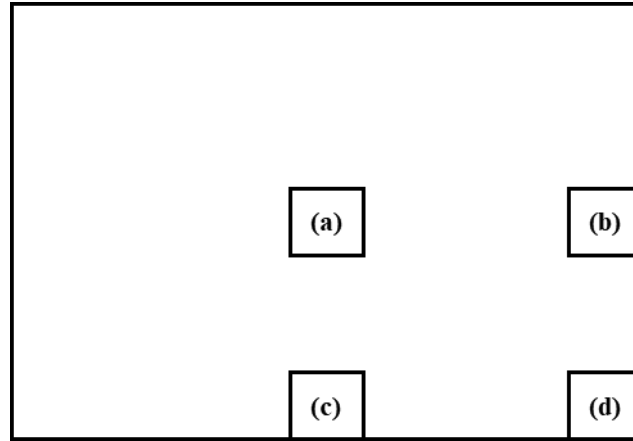
Figure 3. Positions used for images acquisition: (a) center of image, (b) edge on the horizontal axis of image, (c) edge on the vertical axis of image and (d) corner of image.

The data was analyzed to obtain three different parameters: length, area, and projected volume of the squares. The length of the square (in pixels) was obtained both for the RGB image (except for CamBoard Pico Flexx) and the depth image. For the RGB images, a manual measure process was performed, using the Image Viewer application from MATLAB R218a. An algorithm for pre-processing the depth image was developed, following the steps shown on Figure 4.

After the pre-processing step, the dimensions of the foam board square were automatically acquired. To measure both the length and the area of the square, the image was first transformed into binary. The maximum sum of the columns on the image was collected as being the length in pixels and, then, the total sum of the image was acquired, obtaining the area of the square, in pixels.

To measure the projected volume (cube) of the square being analyzed (e.g. a cube of 10 x 10 x 10 cm for the 10 x 10 cm square), the pre-processed image was used to obtain values of the third dimension of the square. This was performed by subtracting the image from the theoretical distance from the base of the cube to the camera (Figure 5). After obtaining the values of depth for each pixel of the theoretical cube, these values were added to obtain the volume of the cube, in pixel cm.

The length ratio, in pixel cm^{-1}, was calculated dividing the length, in pixels, obtained for both RGB (when available) and depth images, by the actual length of the foam board square (either 10, 20 or 30 cm). Furthermore, the area ratio, in px cm^{-2}, was also calculated by dividing the area obtained on the depth image (in pixels) by the actual area of the squares (either 100, 400 or 900 cm²).

These ratios were analyzed using the General Linear Procedure (proc GLM) of SAS software, testing the effects of the use of different positions (center, edge on the horizontal axis of the image, edge on the vertical axis of the image and corner) and different sizes (10 x 10 cm, 20 x 20 cm and 30 x 30 cm) of foam board squares used. Then, regression models were generated for length ratio (px cm-1) versus distance, and for area ratio (px cm^{-2}) versus distance.

Unit transformation equations were developed in order to eliminate the need for the presence of an object with predetermined size to acquire dimensions on an image, as has been used by several authors (Philips & Dawson, 1936; Zaragoza, 2009). To obtain these equations, the metric unit (either cm or cm²) from the regression models developed was isolated.
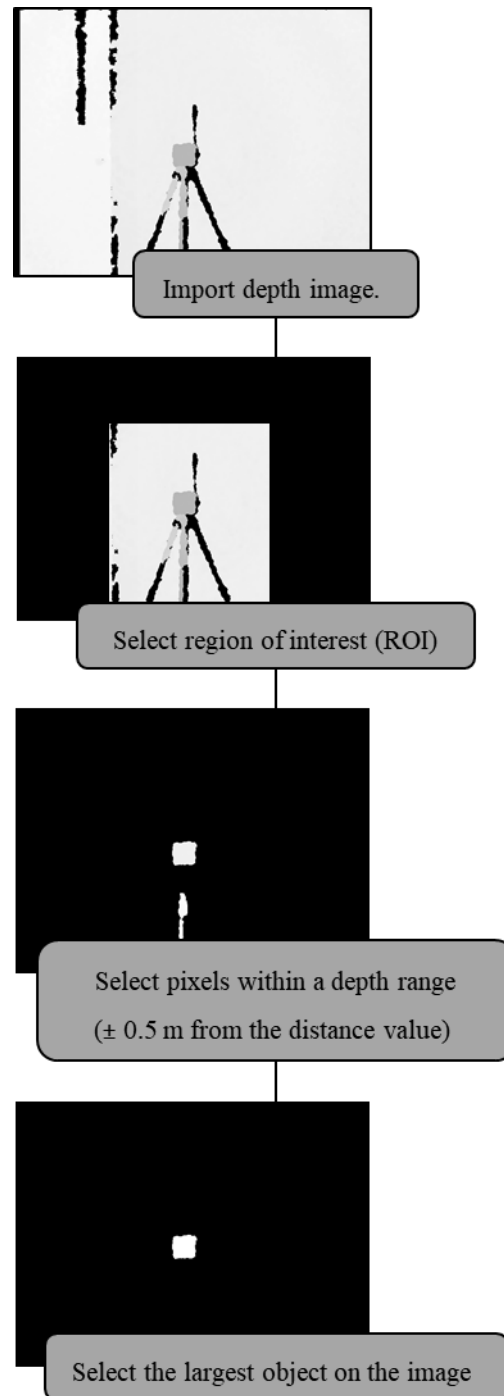
Figure 4. Algorithm for the selection of the foam board square in the image.
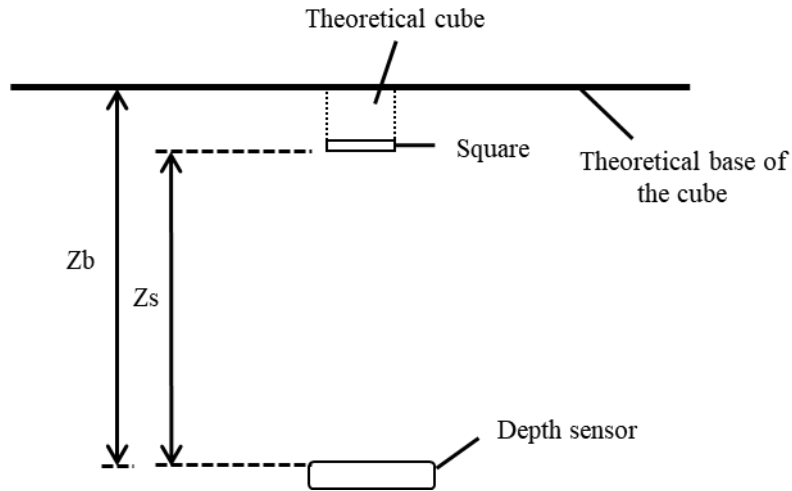
Figure 5. Top-view diagram of the positioning of the depth cameras and the object being analyzed for the calculation of the volume of the theoretical cube with the same size of the square being analyzed.

3.2.3 Maximum useful distance

Five depth and RGB (except CamBoard Pico Flexx-only depth images were collected) images of foam board squares were collected at distances ranging from 1.0 to 20.0 m, every 1.0 m, both indoors and outdoors. For distances 1.0- 10.0 m, a 30 by 30 cm square was used, while a 60 by 60 cm square was used from 11.0 – 20.0 cm. The squares were placed at the center of the image with a tripod (Figure 6).

The foam board square on each image was selected using the algorithm shown on Fig. 4. The values of distance from camera to square were averaged. The residuals between actual distance and camera-provided distance were calculated and a regression model of residuals versus actual distance was calculated when possible (e.g. when the square was within the acquisition range of the camera). The maximum distance of useful data (image with no missing regions and reliable distance date) for each camera was recorded.
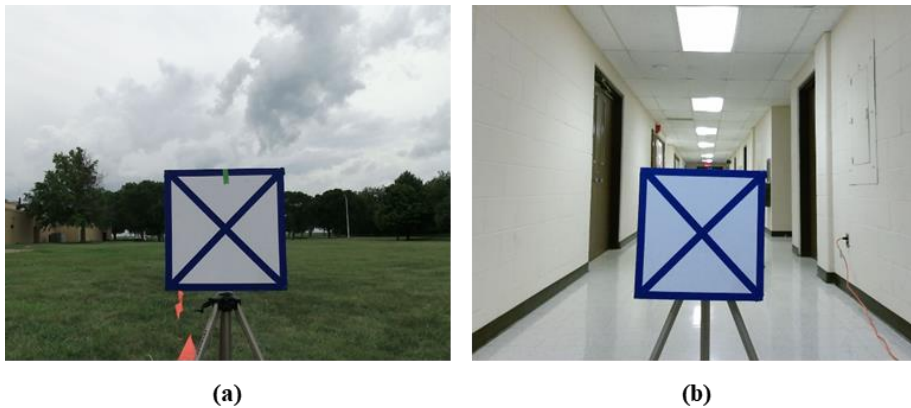

Figure 6. Outdoor (a) and Indoor (b) data collection.

3.2.4 Animal phenotypic data evaluation

Top-view images on fifteen grow-finish pigs randomly sampled at three nominal ages: 8, 12, and 16 weeks old (five animals at each age). A balance of barrows and gilts (Landrace and Yorkshire cross) during each measurement period was evaluated. A total of five depth and RGB (except CamBoard Pico Flexx) images from each type of camera was collected. The cameras were mounted on a bracket above the scale and images were collected as the animals were being weighed (Figure 7). Weights and pigs' identification numbers were manually recorded.

(a) **(b)**

Figure 7. Mass and images were captured on individual pigs using a standard swine scale (b) and five different depth cameras. The cameras were mounted to the wall directly above the center of the scale (a).

The images were processed and analyzed using methods proposed by Condotta et al. (2018a) and Condotta et al. (2018b) to acquire the pig's projected volume (px cm) (Figure 8). The unit was transformed (from px cm to cm³) using equations developed on the second experiment. Linear regressions of mass (kg) versus volume (cm³) were generated for each of the cameras used.
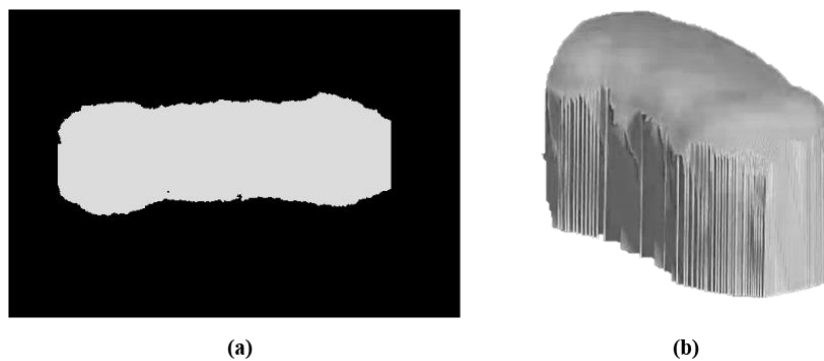

(a) **(b)**

Figure 8. (a) Top-view image of pig without head and tail regions. (b) Projected volume of the animal.

3.3 Results and Discussion

3.3.1 Distance accuracy and repeatability

The average values of distance obtained for the region of the wall in the picture, as well as their respective standard deviations are shown in Table 2. The result of the Efroymson's algorithm showed that the behavior of different cameras of the same type is the same for cameras that use the time-of-flight (ToF) principle, CamBoard Pico Flexx (P = 0.18710) and Microsoft Kinect v.2 (P = 0.70697), but different for the other types of cameras, Intel® RealSense™ D435 (P = 0.2538), Microsoft Kinect v.1 (P = 0.00002) and ZED Stereo Camera (P = 0.00007). From Table 2 it can be notice that there is an increase in the standard deviation with increasing distance from sensor to wall (Figure 9), corroborating with the data obtained by Khoshelham & Elberink (2012).

Table 2. Average distances (m) and standard deviation (m) obtained by five depth cameras, for the five analyzed distances with their respective standard deviations. One hundred and twenty-one points were used for each image to gather each value, and three cameras of each type were used.

Camera	Distances from sensor to wall (m)					P-value
	1.00	1.50	2.00	2.50	3.00	
CamBoard Pico Flexx	0.99 ± 0.001	1.48 ± 0.002	1.99 ± 0.003	2.50 ± 0.004	3.00 ± 0.006	0.18710
Intel® RealSense™ D435	0.99 ± 0.002	1.47 ± 0.012	1.97 ± 0.022	2.46 ± 0.035	2.97 ± 0.036	0.02538
Microsoft Kinect v.1	0.99 ± 0.002	1.49 ± 0.003	1.99 ± 0.006	2.49 ± 0.008	3.00 ± 0.013	0.00002
Microsoft Kinect v.2	1.00 ± 0.001	1.50 ± 0.001	2.01 ± 0.001	2.51 ± 0.002	3.01 ± 0.003	0.70697
ZED Stereo Camera	0.99 ± 0.001	1.48 ± 0.001	1.99 ± 0.002	2.48 ± 0.004	2.99 ± 0.003	0.00007

For Intel RealSense camera it was observed a higher standard deviation when compared with the other cameras. This is probably due to the lack of consistency between cameras, as soon as the standard errors between the three cameras varied from 0.002 to 0.004 at 1.00 m, from 0 to 0.37 at 1.50 m, from 0 to 0.044 at 2.00 m, from 0 to 0.62 at 2.50 m, and from 0.024 to 0.046 at 3.00 m with no visible best camera, however, one cameras was consistently the poorest performing. The second set of testing data was collected on the worst performing camera to ensure the errors were not acquisition errors, but the values were similar to the first acquisition. Even when not using the worst out of the three cameras, the average errors of the two other cameras were still close to the average of all three cameras together and, therefore, this did not interfere on the discussion of the results.
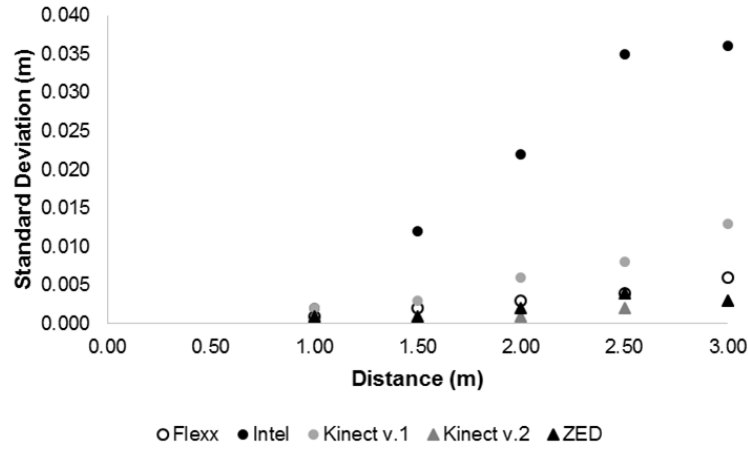
Figure 9. Curves of standard deviation (m) of distance data obtained for five depth cameras (CamBoard Pico Flexx, Intel® RealSense™ D435, Microsoft Kinect v.1, Microsoft Kinect v.2, ZED Stereo Camera) versus the distance between sensor and wall (m).

3.3.2 Dimension accuracy and repeatability

Unit transformation equations were developed from regression models between the area (px cm^{-2}) and length (px cm^{-1}) ratios and the distance (m) from the camera to the foam board square. To transform px to cm, the equations are on the form shown by eq. (2), and, to transform px to cm², the equations are on the form shown by eq. (3). Equations for transformation from depth images and from color images (when available) were developed. Table 3 contains the coefficients of these equations for depth images and Table 4, for color images.

$$l_{cm} = l_{px} \times a \times Z^b \qquad (2)$$

where:

l_{cm} = length, in cm;

l_{px} = length, in pixels;

Z = Distance from depth camera to object being measured (m);

a = coefficient;

b = coefficient.

There is also the possibility of using the data provided on the depth map to calculate the volume of objects. This approach also raises the need for conversion of units, since the volume is calculated by the sum of the distance data from object to its support surface ('height of the object') for the whole object area. As the distance data provided by the sensors are in cm and the area of the object is given in number of pixels, the volume is retrieved in an unwanted unit (px cm). Another problem is the fact that the area of the object in the image varies with its distance from the sensor. This generates the need for correction of the value obtained to perform any comparison between volumes. In other words, for the same object, different values of volumes, lengths and areas can be acquired if the distance from the sensor varies. As what changes to the calculation of the volume is the area of the object and not its depth (distance between the square and the wall), this value can be adjusted using eq. (3), obtained for correcting the area.

$$S_{cm^2} = S_{px} \times a \times Z^b \tag{3}$$

where:

S_{cm^2} = area, in cm²;

S_{px} = area, in pixels;

Z = Distance from depth camera to object being measured (m);

a = coefficient;

b = coefficient.

Testing the effects of using different sizes of foam board squares on the length (px cm⁻¹) and area (px cm⁻²) ratios, showed (Table 5) difference for the 10 cm x 10 cm square for all cameras, except for the acquisition of the area ratio with CamBoard Pico Flexx (PMD Technologies). That could be explained by the fact that very small objects are more impacted from edge deformation effect, as indicated by Gottfried et al. (2011). Microsoft Kinect v.1 showed difference between all sizes of squares used for both length ratio and area ratio, and ZED Stereo Camera (StereoLabs) showed differences between all sizes of square used when measuring length ratio. This could indicate that a square of 20 x 20 cm is still too small for these cameras and suffer from edge effect.

Table 3. Coefficients a and b for unit transformation equations from px to cm (length) and from px to cm² (area) on depth images provided by five depth cameras.

	Length coefficients[1]		R²	Area coefficients[2]		R²
Camera	**a**	**b**		**a**	**b**	
CamBoard Pico Flexx	0.513	0.915	0.993	0.264	1.914	0.998
Intel® RealSense™ D435	0.141	0.875	0.912	0.023	2.004	0.853
Microsoft Kinect v.1	0.165	0.914	0.980	0.029	1.899	0.988
Microsoft Kinect v.2	0.273	0.915	0.996	0.076	1.928	0.977
ZED Stereo Camera	0.063	0.967	0.972	0.005	1.966	0.973

[1] $length_{cm} = length_{px} \times a \times (Distance\ from\ the\ camera)^b$
[2] $area_{cm^2} = area_{px} \times a \times (Distance\ from\ the\ camera)^b$

The test of the effect of the objects' positions in the image (center, edge on the horizontal axis, edge on the vertical axis, and corner) on the length (px cm⁻¹) and area (px cm⁻²) ratios showed (Table 6) a different behavior for each type of camera used. For the ToF cameras (CamBoard Pico Flexx and Microsoft Kinect v.2), all positions present different length ratios. The area ratio for CamBoard Pico Flexx camera is the same between positions 1 and 3 (center and edge on vertical axis) and between positions 2 and 4 (edge on horizontal axis and corner). The area ratio for Microsoft Kinect v.2 is the same between positions 1 and 2, and between 1 and 4; position 3 (edge on vertical axis) differs from the others.

Table 4. Coefficients a and b for unit transformation equations from px to cm (length) on RGB images provided by four depth cameras.

	Length coefficients[1]		R²
Camera	**A**	**b**	
Intel® RealSense™ D435	0.168	1.001	0.990
Microsoft Kinect v.1	0.199	0.966	0.985
Microsoft Kinect v.2	0.096	0.999	0.989
ZED Stereo Camera	0.070	0.999	0.979

[1] $length_{cm} = length_{px} \times a \times (Distance\ from\ the\ camera)^b$

Table 5. Averages and standard errors obtained for length ratio (px cm^{-1}) and area ratio (px cm^{-2}), for the three sizes of square used (10 x 10 cm, 20 x 20 cm and 30 x 30 cm) and five depth cameras.

Camera	Square Size (cm)	Length Ratio (px cm^{-1})	Area Ratio (px cm^{-2})
CamBoard Pico Flexx	10 x 10	1.20 ± 0.01[a]	1.54 ± 0.02
	20 x 20	1.17 ± 0.01[b]	1.54 ± 0.02
	30 x 30	1.17 ± 0.01[b]	1.55 ± 0.02
Intel® RealSense™ D435	10 x 10	4.84 ± 0.06[a]	21.58 ± 0.39[a]
	20 x 20	4.24 ± 0.06[b]	17.65 ± 0.39[b]
	30 x 30	4.11 ± 0.06[b]	16.85 ± 0.39[b]
Microsoft Kinect v.1*	10 x 10	3.92 ± 0.17[a]	15.08 ± 0.14[a]
	20 x 20	3.61 ± 0.17[b]	13.84 ± 0.14[b]
	30 x 30	3.50 ± 0.17[c]	13.16 ± 0.14[c]
Microsoft Kinect v.2*	10 x 10	2.33 ± 0.15[a]	5.56 ± 0.05[a]
	20 x 20	2.19 ± 0.15[b]	5.25 ± 0.05[b]
	30 x 30	2.15 ± 0.15[b]	5.11 ± 0.05[b]
ZED Stereo Camera	10 x 10	9.87 ± 0.07[a]	90.50 ± 1.77[a]
	20 x 20	9.34 ± 0.07[b]	85.43 ± 1.77[b]
	30 x 30	9.04 ± 0.07[c]	83.18 ± 1.77[b]

[a, b, c] Rows for each column, with different superscripts are significantly different ($p<0.05$).
* Microsoft Kinect v.1 showed significant interaction between position and size of the foam board square for length ratio. Microsoft Kinect v.2 showed significant interaction between position and size of the foam board square for both area ratio and length ratio. ZED Stereo Camera showed significant interaction between camera and size of the foam board square for length ratio.

For acquiring length ratio with Intel® RealSense™ D435, position 1 (center) differs from the others, position 3 (edge on vertical axis) has the same effect as positions 2 (edge on horizontal axis) and 4 (corner). The effect of positions on the area ratio for this camera was the same presented by Microsoft Kinect v.1 for both length and area ratios, positions 1 and 2 have the same behavior and positions 3 and 4 have the same behavior.

Dutta (2012), showed that the standard deviation of the distance data increase on the corners of the image. Thus, the ideal for data comparison of length and area of objects acquired with depth cameras is positioning them at a fixed region of the image, preferably in the center. If offsets need to be made, the ideal is to make them on the horizontal direction of the image for Intel® RealSense™ D435 and Microsoft Kinect v.1, and on the vertical direction of the image for CamBoard Pico Flexx (PMD Technologies) and Microsoft Kinect v.2; in which the differences are smaller, reducing distortion of values and enabling data comparison. ZED Stereo Camera (StereoLabs) did not present any effect of positions on the length and area ratios acquisition and, thus, the objects can be positioned in any place on the image. CamBoard Pico Flexx (PMD Technologies), Intel® RealSense™ D435, and Microsoft Kinect v.2 showed no significant effect ($p<0.05$) on the length ratio (px cm-1) and on the area ratio (px cm^{-2}) when using different cameras to acquire those dimensions (Table 7).

Microsoft Kinect v.1 camera showed significant interaction between position and size of the foam board square for length ratio (Figure 10a). Microsoft Kinect v.2 showed significant interaction between position and size of the foam board square for both area ratio (Figure 10d) and length ratio (Figure 10c). ZED Stereo Camera showed significant interaction (Figure 10b) between camera and size of the foam board square for length ratio. For both Kinect cameras, it appears that the source of interaction is the 10 x 10 cm foam board square and for the ZED camera it appears that the source is the 30 x 30 cm square.

Table 6. Averages and standard errors obtained for length ratio (px cm^{-1}) and area ratio (px cm^{-2}), for the four positions on image (1 – center, 2 - edge on the horizontal axis, 3 - edge on the vertical axis, 4- corner) and five depth cameras.

Camera	Position	Length Ratio (px cm^{-1})	Area Ratio (px cm^{-2})
CamBoard Pico Flexx	1	1.21 ± 0.01^a	1.69 ± 0.03^a
	2	1.08 ± 0.01^b	1.41 ± 0.03^b
	3	1.28 ± 0.01^c	1.68 ± 0.03^a
	4	1.14 ± 0.01^d	1.40 ± 0.03^b
Intel® RealSense™ D435	1	4.16 ± 0.07^a	16.98 ± 0.45^a
	2	4.38 ± 0.07^b	17.85 ± 0.45^a
	3	4.46 ± 0.07^{bc}	19.60 ± 0.45^b
	4	4.58 ± 0.07^c	20.34 ± 0.45^b
Microsoft Kinect v.1*	1	3.56 ± 0.02^a	13.44 ± 0.17^a
	2	3.61 ± 0.02^a	13.82 ± 0.17^a
	3	3.78 ± 0.02^b	14.48 ± 0.17^b
	4	3.76 ± 0.02^b	14.37 ± 0.17^b
Microsoft Kinect v.2*	1	2.14 ± 0.02^a	5.13 ± 0.06^{ab}
	2	2.09 ± 0.02^b	5.03 ± 0.06^a
	3	2.42 ± 0.02^c	5.86 ± 0.06^c
	4	2.27 ± 0.02^d	5.21 ± 0.06^b
ZED Stereo Camera	1	9.35 ± 3.89	86.70 ± 75.07
	2	9.28 ± 3.77	82.41 ± 67.40
	3	9.46 ± 3.64	86.81 ± 67.09
	4	9.59 ± 3.93	89.56 ± 73.07

[a, b, c, d] Rows for each column of each camera section, with different superscripts are significantly different (p<0.05).
* Microsoft Kinect v.1 showed significant interaction between position and size of the foam board square for length ratio. Microsoft Kinect v.2 showed significant interaction between position and size of the foam board square for both area ratio and length ratio.

Table 7. Averages and standard errors obtained for length ratio (px cm^{-1}) and area ratio (px cm^{-2}), for the three sizes of square used (10 x 10 cm, 20 x 20 cm and 30 x 30 cm) and fifteen depth cameras (three of each type).

Camera	Camera #	Length Ratio (px cm^{-1})	Area Ratio (px cm^{-2})
CamBoard Pico Flexx	1	1.18 ± 0.01	1.55 ± 0.02
	2	1.18 ± 0.01	1.55 ± 0.02
	3	1.18 ± 0.01	1.53 ± 0.02
Intel® RealSense™ D435	1	4.44 ± 0.06	19.29 ± 0.40
	2	4.44 ± 0.06	18.82 ± 0.40
	3	4.30 ± 0.06	17.96 ± 0.40
Microsoft Kinect v.1	1	3.65 ± 0.02^a	13.79 ± 0.14^a
	2	3.66 ± 0.02^a	13.99 ± 0.14^{ab}
	3	3.72 ± 0.02^b	14.30 ± 0.14^b
Microsoft Kinect v.2	1	2.22 ± 0.01	5.29 ± 0.05
	2	2.23 ± 0.01	5.31 ± 0.05
	3	2.23 ± 0.01	5.32 ± 0.05
ZED Stereo Camera*	1	9.84 ± 0.07^a	94.89 ± 1.77^a
	2	9.41 ± 0.07^b	87.97 ± 1.77^b
	3	9.01 ± 0.07^c	76.24 ± 1.77^c

[a, b, c] Rows for each column, with different superscripts are significantly different (p<0.05).
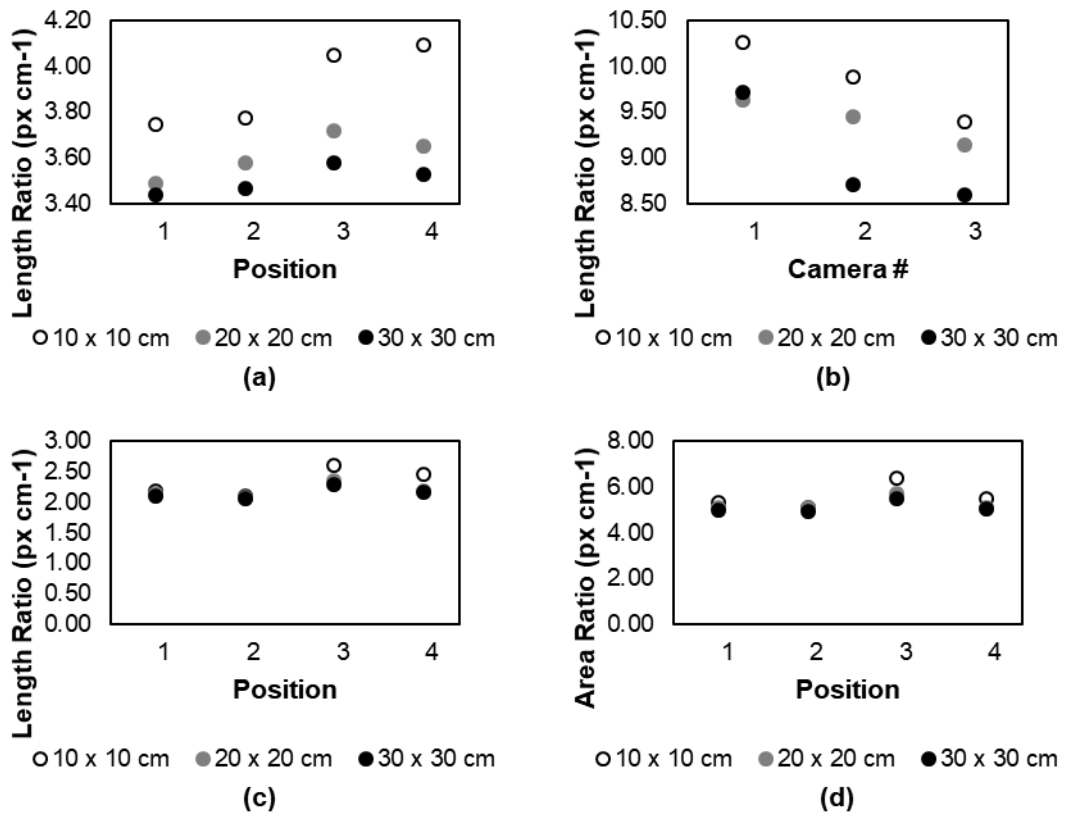* ZED Stereo Camera showed significant interaction between camera and size of the foam board square for length ratio.

Figure 10. Significant interaction of (a) size and position (Microsoft Kinect v.1) affecting length ratio; (b) size and camera (ZED Stereo Camera) affecting length ratio; and size and position (Microsoft Kinect v.2) affecting both (c) length ratio and (d) area ratio.

Figure 11 shows examples of area and length of a 30 x 30 cm foam board square acquired with the five different cameras used in this study and with units corrected using eq. (2) and (3) developed.
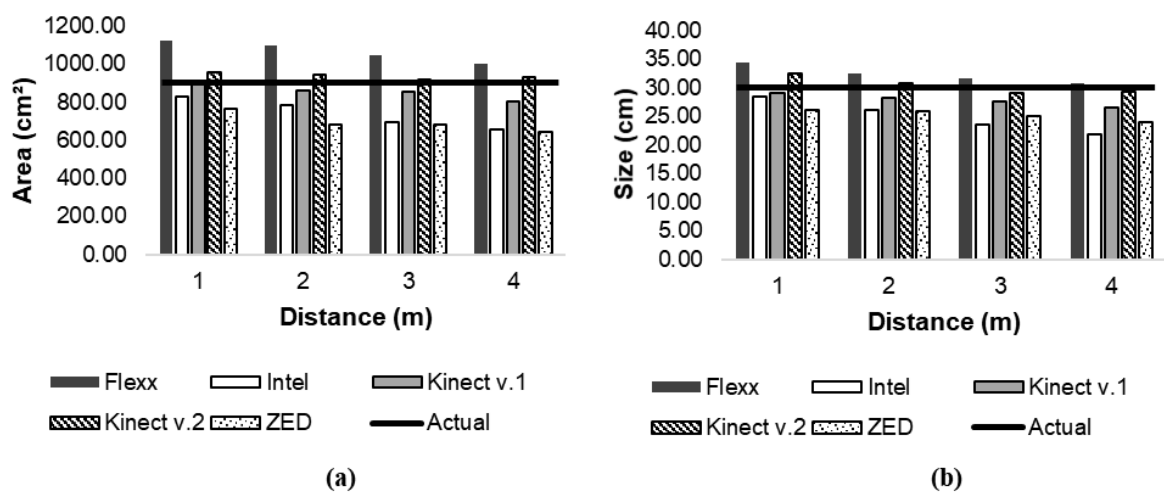

Figure 11. Predicted area and length of foam squares recorded with five depth cameras (CamBoard Pico Flexx, Intel® RealSense™ D435, Microsoft Kinect v.1, Microsoft Kinect v.2, and ZED Stereo Camera).

3.3.3 Maximum useful distance

Average distance from camera to the foam board square (m) was plotted against actual distance (Figures 12a, 13a, 14a, 15a, and 16a) for both indoors and outdoors. Table 8 shows the maximum distance of useful distance data on both environments and classifies the usability of the data for performing measurements outdoors.

The cameras that use stereo vision (Intel® RealSense™ and ZED Stereo Camera) could provide useful data on an outdoor environment up to 12 m (Intel) or 20 m (ZED). For the time-of-flight cameras, some data can be acquired outdoors if the distance from the objects being analyzed is small (1 m for CamBoard Pico Flexx and 2 m for Microsoft Kinect v.2), which prevents their use for autonomous robotic navigation, for example. Kinect v.1 did not present useful data on an outside environment.

Table 8. Maximum distance (m) that depth cameras can acquire data for both indoor and outdoor environments and possibility of performing dimensions' measures outdoor.

Camera	CamBoard Pico Flexx	Intel® RealSense™ D435	Microsoft Kinect v.1	Microsoft Kinect v.2	ZED Stereo Camera
Max. Distance Indoor (m)	7.0	20.0	4.0	7.0	20.0
Max. Distance Outdoor (m)	1.0	20.0	0.0	2.0	20.0
Measurement Outdoor	No	Yes	No	No	Yes

The residuals between actual distance and camera-provided distance were calculated and plotted (Figures 12b, 13b, 14b, 15b, and 16b) against distance. Intel® RealSense™ D435 and ZED Stereo Camera presented the highest residuals. Also, the residuals for these cameras increased with increasing distances, differently from the other cameras that presented a more constant residual with no visible pattern. A power regression model of residuals versus actual distance was calculated for both Intel® RealSense™ D435 and ZED Stereo Camera, which presented residuals with a visually non-random behavior. The power regression equations present form shown in eq. (4), and the coefficients for these equations are presented on Table 9.

$$Res = a \times Z^b \tag{4}$$

where:

Res = residuals (m);

Z = distance from camera to object being measured;

a = coefficient;

b = coefficient.

Table 9. Coefficients of residuals power curves for Intel® RealSense™ D435 and ZED Stereo Camera, indoor and outdoor.

Camera	Coefficients indoor		R²	Coefficients outdoor		R²
	a	b		a	b	
Intel® RealSense™ D435	0539	1.466	0.991	0.049	1.597	0.991
ZED Stereo Camera	0.019	1.766	0.993	0.008	1.049	0.978

(a)

(b)
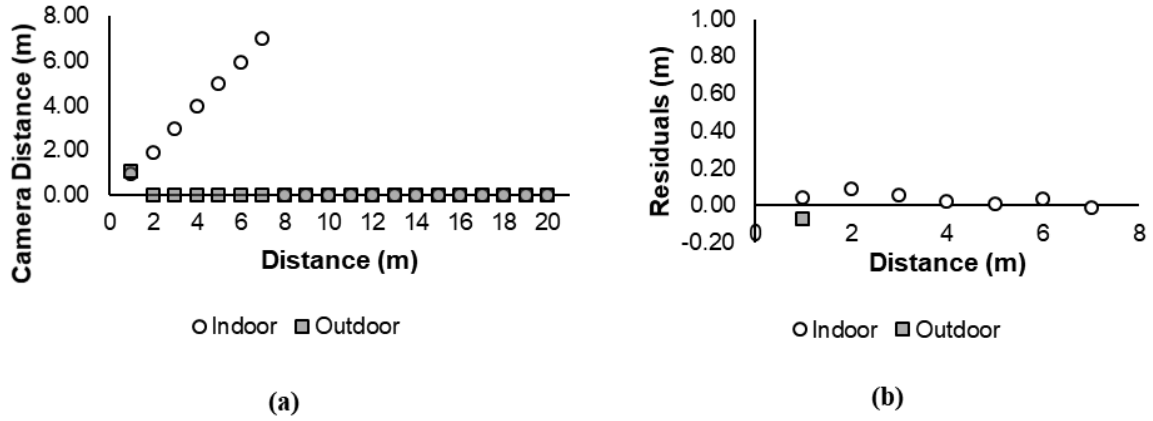
Figure 12. Average distance from camera to the foam board square (m) versus actual distance (m) and residuals of the measurements for CamBoard Pico Flexx (PMD Technologies).

(a)

(b)
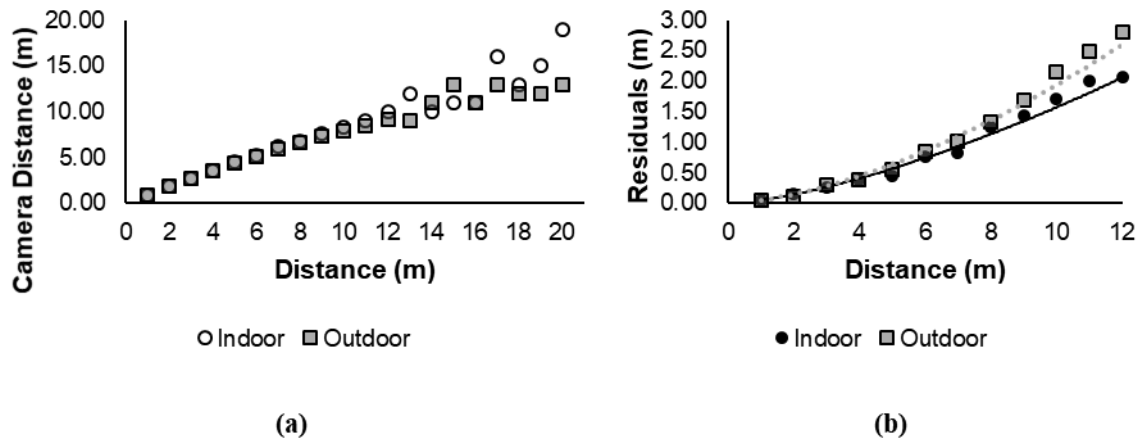
Figure 13. Average distance from camera to the foam board square (m) versus actual distance (m) and residuals of the measurements for Intel® RealSense™ D435.
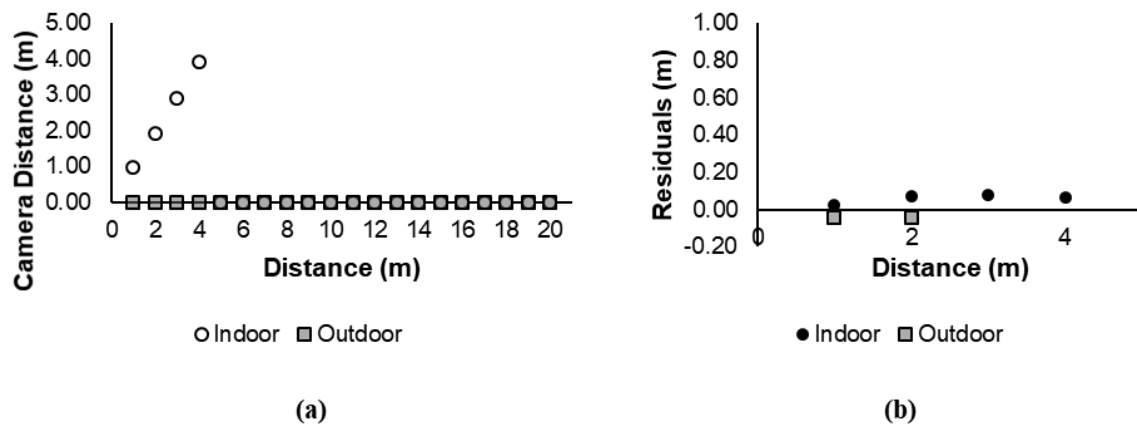
38

Figure 14. Average distance from camera to the foam board square (m) versus actual distance (m) and residuals of the measurements for Microsoft Kinect v.1.
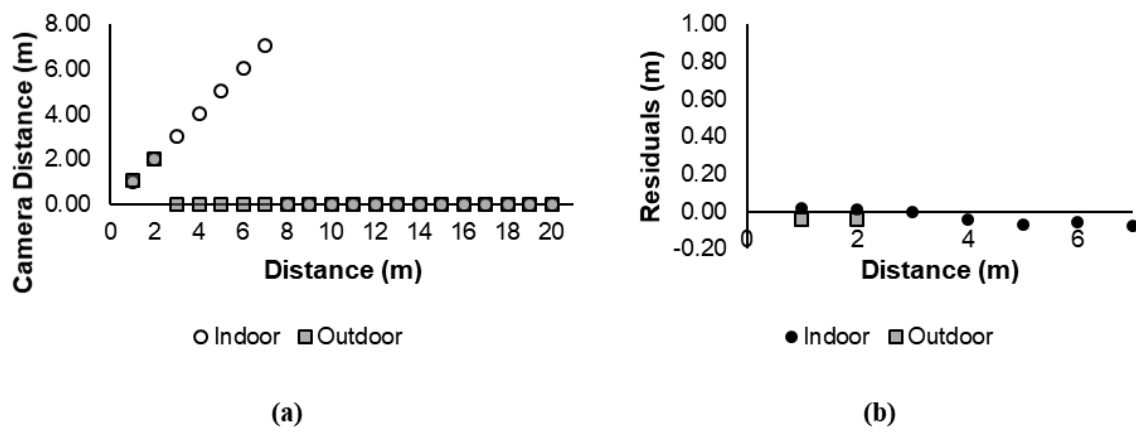

Figure 15. Average distance from camera to the foam board square (m) versus actual distance (m) and residuals of the measurements for Microsoft Kinect v.2.
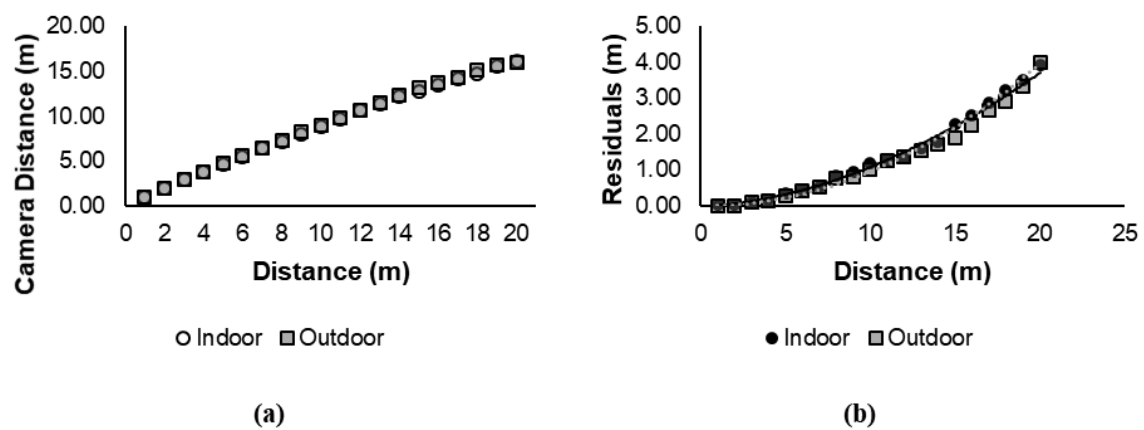

Figure 16. Average distance from camera to the foam board square (m) versus actual distance (m) and residuals of the measurements for ZED Stereo Camera (StereoLabs).

3.3.4 Animal phenotypic data evaluation

Top view images were taken on a group of pigs as they were being weighed. Figure 17 shows the sample of the images captured with all five depth cameras used. As the images are evaluated, all the pigs are easily visible in all the images except the image captured from the ZED Stereo Camera. The main body is easily seen, but the head and the tail are difficult to discern. The image taken with Kinect v.1 has rough edges on the pig. The slightly rough edges are also observed on the image taken with the RealSense camera. Both Time-of-Flight cameras had a clear image, and Kinect v.2 have the smoothest outline of the pigs, probably due to its higher resolution.

The projected volumes (cm³) acquired from the body of the animals, without the head and tail regions, were plotted (Figure 18) against the mass (kg) of the animals. Linear regressions were fitted, and equations were generated with the form presented on eq. 5 and coefficients presented on Table 10. The best correlations between projected volume and mass was obtained for the Time-of-Flight technology (Microsoft Kinect v.2 and CamBoard Pico Flexx). Cameras that use the structured light technology (Intel® RealSense™ and Microsoft Kinect v.1) also had a good correlation (R^2 higher than 0.9) between those two variables. The camera that uses stereo vision-only (StereoLabs ZED) had the lowest correlation ($R^2 = 0.798$) between projected volume and mass. Considering both the shapes provided and the depth information, the cameras that use ToF technology would be more advisable to be used indoor applications, such as animal phenotyping, followed by cameras that use structured light technology.

$$V = a \times M + b \tag{5}$$

where:

V = volume, in cm³;

M = mass, in kg;

a = coefficient;

b = coefficient.

Table 10. Coefficients *a* and *b*, and determination coefficient (R^2) of linear regression equations.

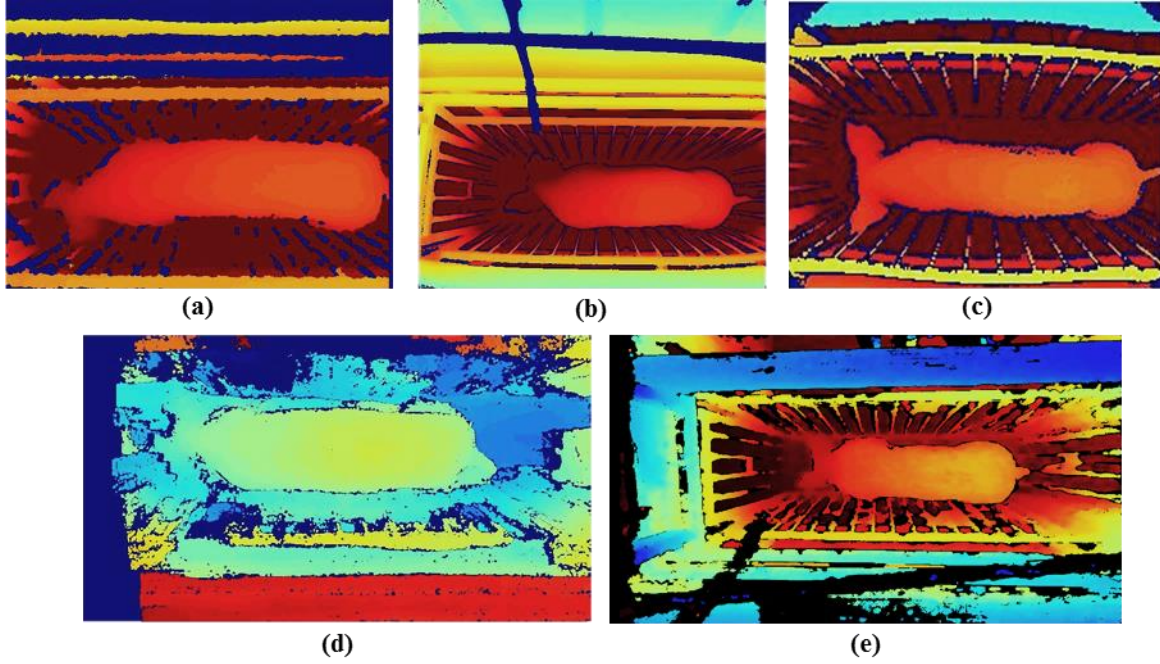| Camera	Coefficients a	b	R²
CamBoard Pico Flexx	12.815	125.990	0.960
Intel® RealSense™ D435	16.791	111.460	0.953
Microsoft Kinect v.1	14.110	34.976	0.901
Microsoft Kinect v.2	13.470	36.439	0.979
ZED Stereo Camera	6.065	350.540	0.798

Figure 17. Depth images acquired from the pigs for all five cameras used: (a) Microsoft Kinect v.1, (b) Microsoft Kinect v.2, (c) CamBoard Pico Flexx (PMD Technologies), (d) ZED Stereo camera (StereoLabs) and (e) Intel® RealSense™ Depth Camera D435.

Figure 18. Linear regressions of volume versus mass obtained with 5 different depth cameras: (a) Microsoft Kinect v.1, (b) Microsoft Kinect v.2, (c) CamBoard Pico Flexx (PMD Technologies), (d) ZED Stereo camera (StereoLabs) and (e) Intel® RealSense™ Depth Camera D435.
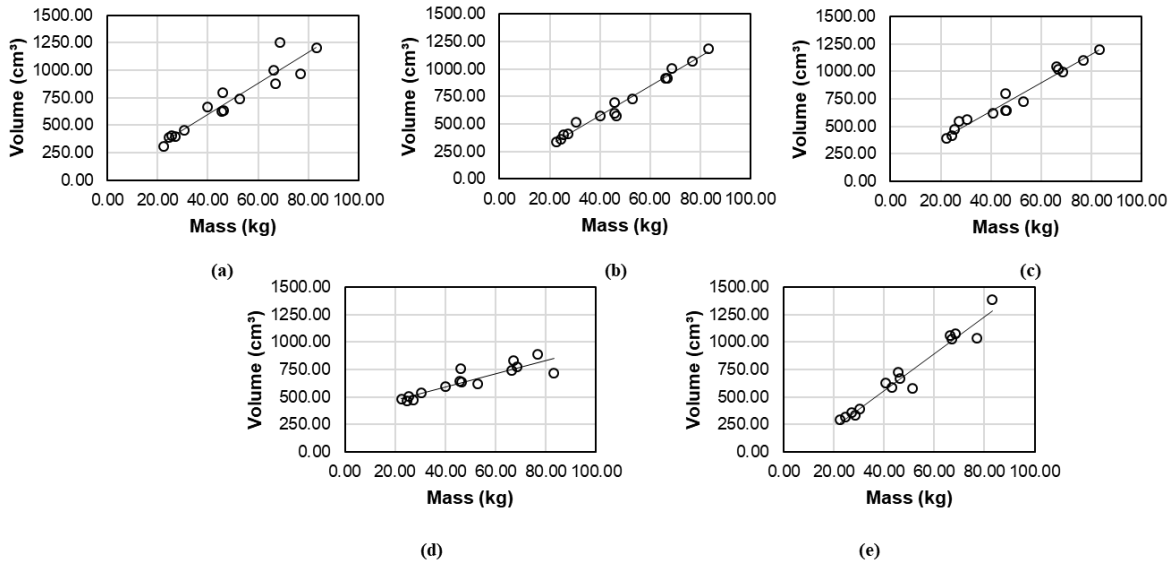
3.4 Conclusions

Low-cost depth-cameras use one or a combination of three technologies: structured light, time-of-flight (ToF), and stereo vision. Five different cameras were tested for their suitability to be used in agriculture applications. Significant camera to camera differences were found for all the cameras ($P<0.05$), except for ToF cameras

(Microsoft Kinect v.2 and CamBoard Pico Flexx). Increases in standard deviation in measurements were found with all camera as the distance between camera and object in-creased; however, Intel® RealSense™ camera had a much larger increase. Time-of-flight cameras had the smallest error between different sizes of objects. All cameras showed some distortion at the edges of the images; however, the ToF cameras had non-readable zones on the corners of the images. Different values of area and length can be acquired with the data provided by depth cameras, for the same object located at different positions in the image. This distortion is greatest in the horizontal axis of the image for the ToF cameras and in the vertical axis for the structured light cameras. The stereo vision-only camera (ZED) did not show any differences between the different positions for dimensions' acquisition. Cameras that use stereo vision technology can be used for outdoors applications. Cameras that use ToF technology, although provide some data on outside environments, should be used outside only if necessary and in a close range (up to 1.0 - 2.0 m). As the variation of distances from sensor to object generates different values of length, area and volume to the same object, it's necessary to standardize these values so that they can be compared. This can be done using the equations 2 and 3, with coefficients provided on tables 3 and 4 proposed in this study. Considering both the shapes provided and the depth information, the cameras that use ToF technology would be more advisable to be used on animal phenotyping, followed by cameras that use structured light technology.

References

Andersen, M. R., Jensen, T., Lisouski, P., Mortensen, A. K., Hansen, M. K., Gregersen, T., & Ahrendt, P. (2012). Kinect Depth Sensor Evaluation for Computer Vision Applications. Electrical and Computer Engineering, Technical, 37. https://doi.org/Technical Report ECE-TR-6

Benavidez, P., & Jamshidi, M. (2011, June). Mobile robot navigation and target tracking system. In 2011 6th International Conference on System of Systems Engineering (pp. 299-304). IEEE.

Berkovic, G., & Shafir, E. (2012). Optical methods for distance and displacement measurements. Advances in Optics and Photonics, 4(4), 441. https://doi.org/10.1364/AOP.4.000441

Chang, Y. J., Chen, S. F., & Chuang, A. F. (2011). A gesture recognition system to transition autonomously through vocational tasks for individuals with cognitive impairments. Research in developmental disabilities, 32(6), 2064-2068.

Chang, Y. J., Chen, S. F., & Huang, J. D. (2011). A Kinect-based system for physical rehabilitation: A pilot study for young adults with motor disabilities. Research in developmental disabilities, 32(6), 2566-2570.

Condotta, I. C. F. S., Brown-Brandl, T. M., Silva-Miranda, K. O., & Stinn, J. P. (2018). Evaluation of a depth sensor for mass estimation of growing and finishing pigs. Biosystems Engineering, 173. https://doi.org/10.1016/j.biosystemseng.2018.03.002

Correa, D. S. O., Sciotti, D. F., Prado, M. G., Sales, D. O., Wolf, D. F., & Osorio, F. S. (2012, May). Mobile robots navigation in indoor environments using kinect sensor. In 2012 Second Brazilian Conference on Critical Embedded Systems (pp. 36-41). IEEE.

Draper, N. R., & Smith, H. (2014). Applied regression analysis (Vol. 326). John Wiley & Sons.

Dutta, T. (2012). Evaluation of the KinectTM sensor for 3-D kinematic measurement in the workplace. Applied Ergonomics, 43(4), 645–649. https://doi.org/10.1016/j.apergo.2011.09.011

Efroymson, M. A. (1960). Multiple regression analysis. Mathematical methods for digital computers, 191-203.

Ganganath, N., & Leung, H. (2012, January). Mobile robot localization using odometry and kinect sensor. In 2012 IEEE International Conference on Emerging Signal Processing Applications (pp. 91-94). IEEE.

Gottfried, J., Fehr, J., & Garbe, C. S. (2011). Advances in Intelligent Computing, 687(January 2011). https://doi.org/10.1007/978-981-10-8974-9

Guo, H., Ma, X., Ma, Q., Wang, K., Su, W., & Zhu, D. H. (2017). LSSA_CAU: An interactive 3d point clouds analysis software for body measurement of livestock with similar forms of cows or pigs. Computers and Electronics in Agriculture, 138, 60–68. https://doi.org/10.1016/j.compag.2017.04.014

Hao, G., & Shengli, Z. (2014). 基于点云采集设备的奶牛体尺指标测量. 116–122.

Hernandez-Lopez, J. J., Quintanilla-Olvera, A. L., López-Ramírez, J. L., Rangel-Butanda, F. J., Ibarra-Manzano, M. A., & Almanza-Ojeda, D. L. (2012). Detecting objects using color and depth segmentation with Kinect sensor. Procedia Technology, 3, 196-204.

Izadi, S., Kim, D., Hilliges, O., Molyneaux, D., Newcombe, R., Kohli, P., ... & Fitzgibbon, A. (2011, October). KinectFusion: real-time 3D reconstruction and interaction using a moving depth camera. In *Proceedings of the 24th annual ACM symposium on User interface software and technology* (pp. 559-568). ACM.

Keselman, L., Woodfill, J. I., Grunnet-Jepsen, A., & Bhowmik, A. (2017). Intel RealSense Stereoscopic Depth Cameras. https://doi.org/10.1109/CVPRW.2017.167

Khoshelham, K., & Elberink, S. O. (2012). Accuracy and resolution of kinect depth data for indoor mapping applications. Sensors, 12(2), 1437-1454.

Kongsro, J. (2014). Estimation of pig weight using a Microsoft Kinect prototype imaging system. Computers and Electronics in Agriculture, 109, 32–35. https://doi.org/10.1016/j.compag.2014.08.008

Kulikov, V. A., Khotskin, N. V., Nikitin, S. V., Lankin, V. S., Kulikov, A. V., & Trapezov, O. V. (2014). Application of 3-D imaging sensor for tracking minipigs in the open field test. Journal of Neuroscience Methods, 235, 219–225. https://doi.org/10.1016/j.jneumeth.2014.07.012

Lao, F., Brown-Brandl, T., Stinn, J. P., Liu, K., Teng, G., & Xin, H. (2016). Automatic recognition of lactating sow behaviors through depth image processing. Computers and Electronics in Agriculture, 125, 56–62. https://doi.org/10.1016/j.compag.2016.04.026

Lee, S., Kim, J., Lim, H., & Ahn, S. C. (2016). Surface reflectance estimation and segmentation from single depth image of ToF camera. Signal Processing: Image Communication, 47, 452–462. https://doi.org/10.1016/j.image.2016.07.006

Phillips, R. W., & Dawson, W. M. (1936). A study of methods for obtaining measurements of swine. Journal of Animal Science, 1936(1), 93-99.

Stavrakakis, S., Li, W., Guy, J. H., Morgan, G., Ushaw, G., Johnson, G. R., & Edwards, S. A. (2015). Validity of the Microsoft Kinect sensor for assessment of normal walking patterns in pigs. Computers and Electronics in Agriculture, 117, 1–7. https://doi.org/10.1016/j.compag.2015.07.003

Wang, Y., Yang, W., Winter, P., & Walker, L. (2008). Walk-through weighing of pigs using machine vision and an artificial neural network. Biosystems Engineering, 100(1), 117–125. https://doi.org/10.1016/j.biosystemseng.2007.08.008

Zaragoza, L. E. O. (2009). Evaluation of the accuracy of simple body measurements for live weight prediction in growing-finishing pigs. MSc. Diss. Univ. of Illinois, Urbana, Illinois.

Zhang, S. (2018). High-speed 3D shape measurement with structured light methods: A review. Optics and Lasers in Engineering, 106(December 2017), 119–131. https://doi.org/10.1016/j.optlaseng.2018.02.017

Zhu, Q., Ren, J., Barclay, D., McCormack, S., & Thomson, W. (2015). Automatic animal detection from Kinect sensed images for livestock monitoring and assessment. Proceedings - 15th IEEE International Conference on Computer and Information Technology, CIT 2015, 14th IEEE International Conference on Ubiquitous Computing and Communications, IUCC 2015, 13th IEEE International Conference on Dependable, Autonomic and Se, 1154–1157. https://doi.org/10.1109/CIT/IUCC/DASC/PICOM.2015.172

Andersen, M. R., Jensen, T., Lisouski, P., Mortensen, A. K., Hansen, M. K., Gregersen, T., & Ahrendt, P. (2012). Kinect Depth Sensor Evaluation for Computer Vision Applications. *Electrical and Computer Engineering, Technical*, 37. https://doi.org/Technical Report ECE-TR-6

Anil, S. S., Anil, L., & Deen, J. (2009). *Javma.235.6.734 (1). 235*(6).

Berkovic, G., & Shafir, E. (2012). Optical methods for distance and displacement measurements. *Advances in Optics and Photonics*, *4*(4), 441. https://doi.org/10.1364/AOP.4.000441

Charette, R., Bigras-Poulin, M., & Martineau, G. P. (1996). Body condition evaluation in sows. *Livestock Production Science*, *46*(2), 107–115. https://doi.org/10.1016/0301-6226(96)00022-X

Condotta, I. C. F. S., Brown-Brandl, T. M., Silva-Miranda, K. O., & Stinn, J. P. (2018). Evaluation of a depth sensor for mass estimation of growing and finishing pigs. *Biosystems Engineering*, *173*. https://doi.org/10.1016/j.biosystemseng.2018.03.002

Condotta, I. C. F. S., Brown-Brandl, T. M., Silva-Miranda, K. O., & Stinn, J. P. (2018). Evaluation of a depth sensor for mass estimation of growing and finishing pigs. *Biosystems Engineering*, 2–9. https://doi.org/10.1016/j.biosystemseng.2018.03.002

De Rensis, F., Gherpelli, M., Superchi, P., & Kirkwood, R. N. (2005). Relationships between backfat depth and plasma leptin during lactation and sow reproductive performance after weaning. *Animal Reproduction Science*, *90*(1–2), 95–100. https://doi.org/10.1016/j.anireprosci.2005.01.017

Eissen, J. J., Kanis, E., & Kemp, B. (2000). Sow factors affecting voluntary feed intake during lactation. *Livestock Production Science*, *64*(2–3), 147–165. https://doi.org/10.1016/S0301-6226(99)00153-0

Esbenshade, K. L., Britt, J. H., Armstrong, J. D., Toelle, V. D., & Stanislaw, C. M. (1986). Body condition of sows across parities and relationship to reproductive performance. *Journal of Animal Science*, *62*(5), 1187–1193. https://doi.org/10.2527/jas1986.6251187x

Grégoire, J., Bergeron, R., D'Allaire, S., Meunier-Salaün, M.-C., & Devillers, N. (2013). Assessment of lameness in sows using gait, footprints, postural behaviour and foot lesion analysis. *Animal*, *7*(07), 1163–1173. https://doi.org/10.1017/s1751731113000098

Guo, H., Ma, X., Ma, Q., Wang, K., Su, W., & Zhu, D. H. (2017). LSSA_CAU: An interactive 3d point clouds analysis software for body measurement of livestock with similar forms of cows or pigs. *Computers and Electronics in Agriculture*, *138*, 60–68. https://doi.org/10.1016/j.compag.2017.04.014

Guo, Y., Zhu, W., Jiao, P., & Chen, J. (2014). Foreground detection of group-housed pigs based on the combination of Mixture of Gaussians using prediction mechanism and threshold segmentation. *Biosystems Engineering*, *125*, 98–104. https://doi.org/10.1016/j.biosystemseng.2014.07.002

Kashiha, M., Bahr, C., Ott, S., Moons, C. P. H., Niewold, T. A., Ödberg, F. O., & Berckmans, D. (2014). Automatic weight estimation of individual pigs using image analysis. *Computers and Electronics in Agriculture*, *107*, 38–44. https://doi.org/10.1016/j.compag.2014.06.003

Keselman, L., Woodfill, J. I., Grunnet-Jepsen, A., & Bhowmik, A. (2017). *Intel RealSense Stereoscopic Depth Cameras*. https://doi.org/10.1109/CVPRW.2017.167

Kim, K. H., Hosseindoust, A., Ingale, S. L., Lee, S. H., Noh, H. S., Choi, Y. H., … Chae, B. J. (2016). Effects of gestational housing on reproductive performance and behavior of sows with different backfat thickness. *Asian-Australasian Journal of Animal Sciences*, *29*(1), 142–148. https://doi.org/10.5713/ajas.14.0973

Knauer, M., Stalder, K., Baas, T., Johnson, C., & Karriker, L. (2012). Physical Conditions of Cull Sows Associated with On-Farm Production Records. *Open Journal of Veterinary Medicine*, *02*(03), 137–150. https://doi.org/10.4236/ojvm.2012.23023

Knauer, M., Stalder, K. J., Karriker, L., Baas, T. J., Johnson, C., Serenius, T., … McKean, J. D. (2007). A descriptive survey of lesions from cull sows harvested at two Midwestern U.S. facilities. *Preventive Veterinary Medicine*, *82*(3–4), 198–212. https://doi.org/10.1016/j.prevetmed.2007.05.017

Knauer, M. T., & Baitinger, D. J. (2015). The sow body condition caliper. *Applied Engineering in Agriculture*, *31*(2), 175–178. https://doi.org/10.13031/aea.31.10632

Kongsro, J. (2014). Estimation of pig weight using a Microsoft Kinect prototype imaging system. *Computers and Electronics in Agriculture*, *109*, 32–35. https://doi.org/10.1016/j.compag.2014.08.008

Kulikov, V. A., Khotskin, N. V., Nikitin, S. V., Lankin, V. S., Kulikov, A. V., & Trapezov, O. V. (2014). Application of 3-D imaging sensor for tracking minipigs in the open field test. *Journal of Neuroscience Methods*, *235*, 219–225. https://doi.org/10.1016/j.jneumeth.2014.07.012

Kuzuhara, Y., Kawamura, K., Yoshitoshi, R., Tamaki, T., Sugai, S., Ikegami, M., … Yasuda, T. (2015). A preliminarily study for predicting body weight and milk properties in lactating Holstein cows using a three-dimensional camera system. *Computers and Electronics in Agriculture*, *111*, 186–193. https://doi.org/10.1016/j.compag.2014.12.020

Lachat, E., Macher, H., Mittet, M. A., Landes, T., & Grussenmeyer, P. (2015). First experiences with kinect V2 sensor for close range 3D modelling. *International Archives of the Photogrammetry, Remote Sensing and Spatial Information Sciences - ISPRS Archives*, *40*(5W4), 93–100. https://doi.org/10.5194/isprsarchives-XL-5-W4-93-2015

Lao, F., Brown-Brandl, T., Stinn, J. P., Liu, K., Teng, G., & Xin, H. (2016). Automatic recognition of lactating sow behaviors through depth image processing. *Computers and Electronics in Agriculture*, *125*, 56–62. https://doi.org/10.1016/j.compag.2016.04.026

Lee, S., Kim, J., Lim, H., & Ahn, S. C. (2016). Surface reflectance estimation and segmentation from single depth image of ToF camera. *Signal Processing: Image Communication*, *47*, 452–462. https://doi.org/10.1016/j.image.2016.07.006

Maes, D. G. D., Janssens, G. P. J., Delputte, P., Lammertyn, A., & De Kruif, A. (2004). Back fat measurements in sows from three commercial pig herds: Relationship with reproductive efficiency and correlation with visual body condition scores. *Livestock Production Science*, *91*(1–2), 57–67. https://doi.org/10.1016/j.livprodsci.2004.06.015

Magowan, E., & McCann, M. E. E. (2006). A comparison of pig backfat measurements using ultrasonic and optical instruments. *Livestock Science*, *103*(1–2), 116–123. https://doi.org/10.1016/j.livsci.2006.02.002

Main, D. C. J., Clegg, J., Spatz, A., & Green, L. E. (2000). Repeatability of a lameness scoring system for finishing pigs. *Veterinary Record*, *147*(20), 574–576. https://doi.org/10.1136/vr.147.20.574

Nalon, E., Conte, S., Maes, D., Tuyttens, F. A. M., & Devillers, N. (2013). Assessment of lameness and claw lesions in sows. *Livestock Science*, *156*(1–3), 10–23. https://doi.org/10.1016/j.livsci.2013.06.003

Ott, S., Moons, C. P. H., Kashiha, M. A., Bahr, C., Tuyttens, F. A. M., Berckmans, D., & Niewold, T. A. (2014). Automated video analysis of pig activity at pen level highly correlates to human observations of behavioural activities. *Livestock Science*, *160*(1), 132–137. https://doi.org/10.1016/j.livsci.2013.12.011

Pezzuolo, A., Guarino, M., Sartori, L., González, L. A., & Marinello, F. (2018). On-barn pig weight estimation based on body measurements by a Kinect v1 depth camera. *Computers and Electronics in Agriculture*, *148*(August 2017), 29–36. https://doi.org/10.1016/j.compag.2018.03.003

Salak-Johnson, J. L., Niekamp, S. R., Rodriguez-Zas, S. L., Ellis, M., & Curtis, S. E. (2007). Space allowance for dry, pregnant sows in pens: Body condition, skin lesions, and performance. *Journal of Animal Science*, *85*(7), 1758–1769. https://doi.org/10.2527/jas.2006-510

Sarbolandi, H., Lefloch, D., & Kolb, A. (2015). Kinect range sensing: Structured-light versus Time-of-Flight Kinect. *Computer Vision and Image Understanding*, *139*, 1–20. https://doi.org/10.1016/j.cviu.2015.05.006

Schofield, C. P. (1990). Evaluation of image analysis as a means of estimating the weight of pigs. *Journal of Agricultural Engineering Research*, *47*(C), 287–296. https://doi.org/10.1016/0021-8634(90)80048-Y

Schofield, C. P., Marchant, J. A., White, R. P., Brandl, N., & Wilson, M. (1999). Monitoring pig growth using a prototype imaging system. *Journal of Agricultural and Engineering Research*, *72*(3), 205–210. https://doi.org/10.1006/jaer.1998.0365

Sell-Kubiak, E. (2015). *Non-genetic variance in pigs: genetic analysis of production and reproduction traits*.

Stavrakakis, S., Li, W., Guy, J. H., Morgan, G., Ushaw, G., Johnson, G. R., & Edwards, S. A. (2015). Validity of the Microsoft Kinect sensor for assessment of normal walking patterns in pigs. *Computers and Electronics in Agriculture*, *117*, 1–7. https://doi.org/10.1016/j.compag.2015.07.003

Wang, Y., Yang, W., Winter, P., & Walker, L. (2008). Walk-through weighing of pigs using machine vision and an artificial neural network. *Biosystems Engineering*, *100*(1), 117–125. https://doi.org/10.1016/j.biosystemseng.2007.08.008

Weber, A., Salau, J., Haas, J. H., Junge, W., Bauer, U., Harms, J., … Thaller, G. (2014). Estimation of backfat thickness using extracted traits from an automatic 3D optical system in lactating Holstein-Friesian cows. *Livestock Science*, *165*(1), 129–137. https://doi.org/10.1016/j.livsci.2014.03.022

Wu, J., Tillett, R., McFarlane, N., Ju, X., Siebert, J. P., & Schofield, P. (2004). Extracting the three-dimensional shape of live pigs using stereo photogrammetry. *Computers and Electronics in Agriculture*, *44*(3), 203–222. https://doi.org/10.1016/j.compag.2004.05.003

Zhang, S. (2018). High-speed 3D shape measurement with structured light methods: A review. *Optics and Lasers in Engineering*, *106*(December 2017), 119–131. https://doi.org/10.1016/j.optlaseng.2018.02.017

Zhu, Q., Ren, J., Barclay, D., McCormack, S., & Thomson, W. (2015). Automatic animal detection from Kinect sensed images for livestock monitoring and assessment. *Proceedings - 15th IEEE International Conference on Computer and Information Technology, CIT 2015, 14th IEEE International Conference on Ubiquitous Computing and Communications, IUCC 2015, 13th IEEE International Conference on Dependable, Autonomic and Se*, 1154–1157. https://doi.org/10.1109/CIT/IUCC/DASC/PICOM.2015.172

4 IMPROVING SOWS' PERFORMANCE: BODY CONDITION SCORE, BACKFAT AND BODY MASS PREDICTION THROUGH DEPTH IMAGE ANALYSIS

Abstract

Observation, control and maintenance of physical condition of sows in acceptable levels is critical to maintain animal welfare and production standards. Early recognition of animals that present atypical physical condition is important to prevent production losses. Currently, the classification of both body condition and lameness is done by subjective methods, thus is dependent on the opinion of the manager, which can generate differences between ratings. As alternatives to these subjective methods of classification, various methods have been proposed to obtain a more objective measure. Body mass can also be an indicative of the physical condition of animals. A way to standardize these measurements would be to automate the process by analyzing images generated by depth cameras. The present work aimed to obtain three characteristics (body condition score, body mass and backfat thickness) of sows using a commercially available depth camera. A multiple linear regression was obtained using the minor axis of the ellipse fitted around sow's body, the width at shoulders, and the angle, of the last rib's curvature to predict body condition. To predict backfat, a multiple linear regression was performed using the height of last rib's curvature, the perimeter of sow's body, the major axis of the ellipse fitted around sow's body, the length from snout to rump, and the predicted body condition score. It was possible to obtain the body mass with a simple linear regression using the projected volume of the sows' body. With these three characteristics it could be possible to have better insights on the physical condition of sows and aid on better and faster management decisions.

Keywords: Precision livestock farming; Time-of-flight; Swine

4.1 Introduction

The observation, control and maintenance of the physical condition of sows in acceptable levels is critical to maintain the animal welfare and production in appropriate standards. The animal welfare assessment protocol for pigs, Welfare Quality® (Quality, 2009), states that good feeding, one of the principles of the animal welfare, is composed of two criteria: absence of prolonged hunger and absence of prolonged thirst. It is proposed to evaluate the first criterion on sows by measuring the body condition of the animals. This is suggested to be done in a subjective method, visually and by touch, classifying the body condition in three levels: level 0 (sow in good condition, with well-developed muscles on the bone), level 1 (thin sow, with bones easily felt; or sow visually obese) and 2 (very thin sow, with the hips and backbone prominent).

It is known that, during pregnancy, each sow should receive a different amount of food according to its body condition. Bigger, older, or skinnier sows should receive higher amounts of food to meet their nutritional needs. Underweight animals present nutritional deficiency, fewer piglets born per litter, and those that are born, can present also nutritional deficiencies and smaller body mass (Eissen et al., 2000). Overweight sows are usually larger than the space provided in the pen, which leads to stress for the animal and may cause piglets' crushing. In addition, these sows have an abnormal development of mammary glands, reducing the amount of milk produced during lactation. Sows that are obese during pregnancy tend to reduce the amount of food ingested during lactation, which also reduces the amount of milk produced (Eissen et al., 2000). These factors can result in economic losses.

Therefore, the early recognition of animals that present physical condition outside the standards is important to prevent production losses. Some authors have been using ratings like those proposed by the Welfare Quality® to assess body condition of sows over the years (Charette et al., 1996; Esbenshade et al., 1986; M. Knauer et al., 2007; M. T. Knauer & Baitinger, 2015; Mark Knauer et al., 2012; Maes et al., 2004; Patience & Thacker, 1989;

Salak-Johnson et al., 2007). As alternatives, various methods have been proposed to obtain a more objective measure.

In the end of the 90's, it was noted (Charette et al., 1996) the need for evaluation of body condition of sows using not only subjective methods of classification, but also more objective values, as body mass, backfat thickness and dimensions of the animal, taking parity into consideration. This type of classification, covering a larger number of variables, was adopted more recently (Sell-Kubiak, 2015) and expanded, using also the duration of the sow's gestation as a factor to be considered.

To reduce the errors with the body condition scoring, one should try to reduce the variation generated by the classification done by different managers. A way of doing that was proposed by Knauer & Baitinger (2015), who developed a caliper that quantifies the angularity from the spinous process to the transverse process of a sow's back and concluded that this instrument can be used as a tool to standardize this classification. Another way to standardize this measurement would be to automate the process by analyzing images generated by depth cameras. This method was used for dairy cows (Kazuhara et al., 2015), obtaining a correlation of 74% between the predicted and actual body condition score. This can indicate the possibility of using this method for sows.

The most used method for acquiring the backfat thickness (De Rensis et al., 2005; Kim et al., 2016; M. T. Knauer & Baitinger, 2015; Maes et al., 2004; Magowan & McCann, 2006) is through ultrasonic probes. One problem with this approach is the difficulty of applying it on an industrial scale since this assessment should be done manually for each animal. Noticing this difficulty in the production of dairy cows, Weber et al. (2014) proposed the use of a depth camera for prediction of their body fat, obtaining a correlation of 96% with the fat thickness measured with ultrasonic probes. This could indicate a possibility of using this method on sows to predict their backfat.

Weighing is a time consuming and stressful practice. To reduce this problem, several authors (Isabella C.F.S. Condotta, Brown-Brandl, Silva-Miranda, & Stinn, 2018; Kongsro, 2014; Ott et al., 2014; Schofield, Marchant, White, Brandl, & Wilson, 1999; Wu et al., 2004) have been using pigs' dimensions data for predicting animal's mass. To replace the scale by an indirect method, both the convenience and the accuracy of the method to be used should be considered. Different methods of obtaining pigs' mass have been tested by many authors (Philips & Dawson, 1936; Zagaroza, 2009). The use of calipers and tape is shown to be effective, but the need to restrict the animals to obtain the data makes this process impracticable on an industrial scale and equivalent to the process of weighing itself.

The use of images to obtain pigs' dimensions is interesting because of its non-invasive approach. Problems with that approach include the fact that the animal's skin and hair colors must be distinct from the environment color, so dark, stained or dirty animals hinder the automation of this approach. A different approach has been used (Kongsro, 2014; Condotta et al., 2018; Pezzuollo et al., 2018), applying depth cameras to obtain pigs' mass (boars and grow-finishing). This approach reduces the problems due to the color of the animals. No approach was made on acquiring sow's mass through depth images.

The present work aims to obtain three characteristics (body condition score, body mass and backfat thickness) of sows using a commercially available depth camera.

4.2 Materials and Methods

The experiment was conducted in a gestating building of the U.S. Meat Animal Research Center, from the Agriculture Research Service-ARS of United States Department of Agriculture – USDA (-98.13° W, 42.52° N).

Animal digital and depth images were collected on a population of sows at four parities, and at two different time-points: on the day of moving to the farrowing building and on the day of moving from the farrowing building. Animal mass was collected on the day of moving from the farrowing building. All animal procedures were performed in compliance with federal and institutional regulations regarding proper animal care practices (FASS, 2010).

4.2.1 Preliminary Study

A preliminary study was conducted to test the calliper proposed by Knauer & Baitinger (2015) and the feasibility of using depth images to obtain a correlation with the values of body condition score (BCS). For that, depth images (Figure 1) of a paper cylinder were acquired and the BCS was obtained with the calliper. The size of the paper cylinder was set to obtain a BCS range from 7 to 21. The cylinder was selected on the image by a depth threshold and its width was acquired in pixels and, then, transformed to cm using eq. 1, proposed on the third chapter of this thesis.
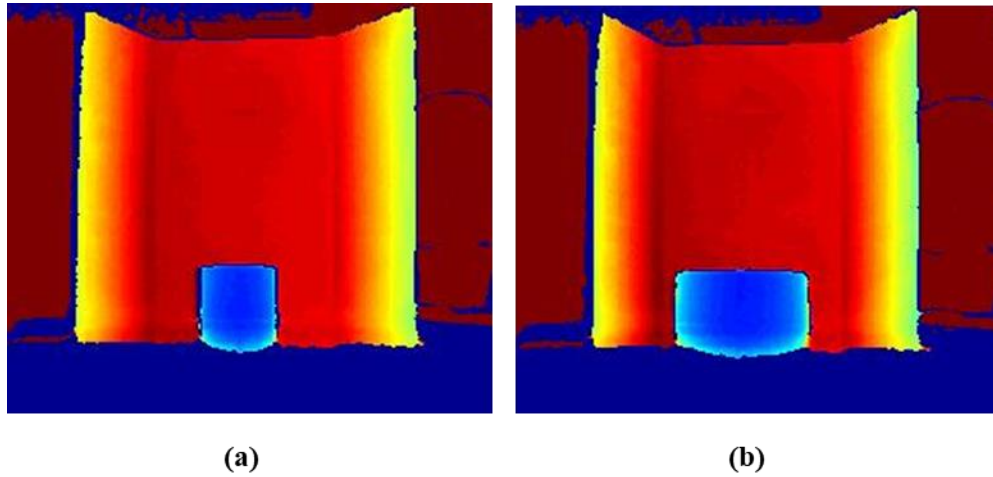

(a)   **(b)**

Figure 1. Depth images of paper cylinder (center of image) with a BCS of 7 (a) and 21 (b).

$$l_{cm} = l_{px} \times 0.273 \times Z_m^{0.915} \tag{1}$$

where:

l_{cm} = length, in cm;

l_{px} = length, in pixels;

Z_m = distance from the camera to the object being analysed, in meters.

4.2.2 Animal Specifics

Two-hundred and twenty-eight sows at four different parities (1, 2, 3, and 4), weighing approximately between 130 and 260 kg, from a rotational Landrace and Yorkshire cross were sampled. The animals were allocated in a gestating building. Animals were sampled at two different time-points: on the day of moving to the farrowing building and on the day of moving from the farrowing building. The first group received a restricted diet and ad libitum water and were housed in a group-pen; while the second group had ad libitum access to both feed and water and were housed in individual crates. Diets were a mix of corn and soybean meal formulated to meet or exceed National Research Council recommendations (NRC, 2012).

4.2.3 Data Acquisition

Microsoft® Kinect Studio program was used to acquire both digital RGB color and depth videos from a commercially available depth camera (Microsoft Kinect® v.2). The program was deployed on a Windows®-based computer for data collection. The camera was positioned above the hallway of the building mounted on the ceiling to take both dorsal color (1920 x 1080 pixels per frame, Figure 2a) and depth videos (512 x 424 pixels per frame, Figure 2b) of the animals while being moved to and from the farrowing building, at approximately 30 frames per second.

Animals were weighed when moving to the gestating building (after farrowing) using a Rice Lake weighing Systems digital weighing scale, that was calibrated by the company and regularly checked with a 50 lb. weight. To acquire the body condition score of animals, the caliper proposed by Knauer & Baitinger (2015) was used as standard (Figure 3). Backfat was acquired on the 10th rib region of the animal using an Ibex EVO with a L6E-3M transductor (E.I. Medical Imaging, Loveland, CO, USA) and the system BioQuant Nova Prime Image (v. 6.9.1, BioQuant Image Analysis Corp., Nashville, TN, USA).
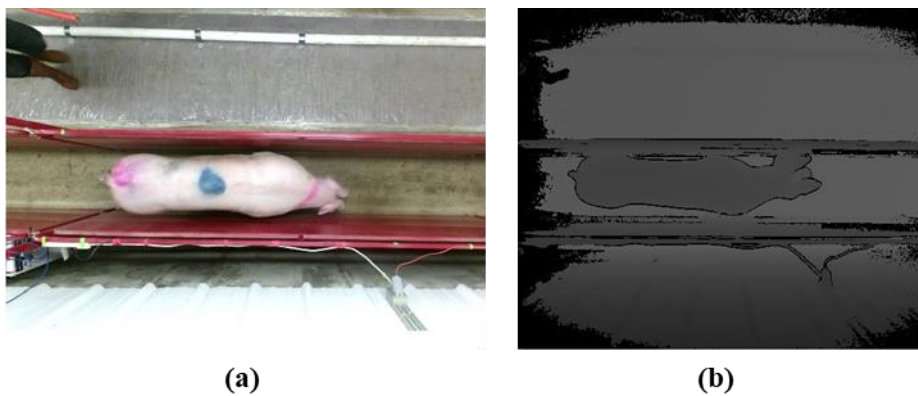

(a)   (b)

Figure 2. Example of (a) color and (b) depth frames acquired.

Figure 3. Body condition score acquired with caliper proposed by Knauer & Baitinger (2015). (b) Backfat acquired with ultrasound probe.

4.2.4 Data Analysis

An algorithm, proposed by Condotta et al. (2018), was used in a numerical computing software (MATLAB, version R2018a) for pre-processing the images, by selecting the animal and removing its head and tail regions. The area, in pixels and the projected volume of the sow's body were acquired (Figure 4). Both top-view cleaned binary images (with and without head and tail regions) were used to acquire the following dimensions on the animals: average height, maximum height (HM), height at shoulders (HS), height at last rib (HR), height at hip (HHp), width at shoulders (WS), width at last rib (WR), width at hip (WH), length from neck to rump (LN), length from shoulders to rump (LS), length from shoulders to hip (LH), length, from snout to rump (L) (Figure 5). Also, an ellipse was fitted on the animals' body (without head region) and its major and minor axis lengths were calculated (Figure 6a). The perimeter of the body region of the animal was also acquired (Figure 6b). All frames of the videos that contained an entire animal were automatically selected and processed and the animals' dimensions were acquired by averaging these frames.
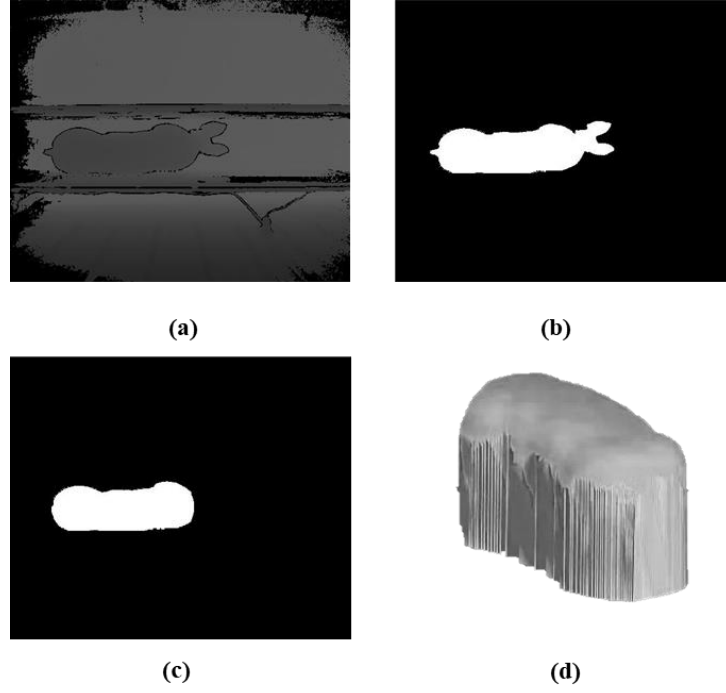
Figure 4. (a) Raw depth image. (b) Cleaned binary image. (c) Cleaned image without head and tail regions, used for calculating the area of the animal. (d) Projected volume of sow's body.

To select the shoulder, hip and last rib regions, the animal was divided into parts, front and back, by the centroid. Then, the widest region on the front of the animal was marked as the shoulders, and the widest region on the back part was marked as the hip. For the last rib, the smallest region on the back was selected.
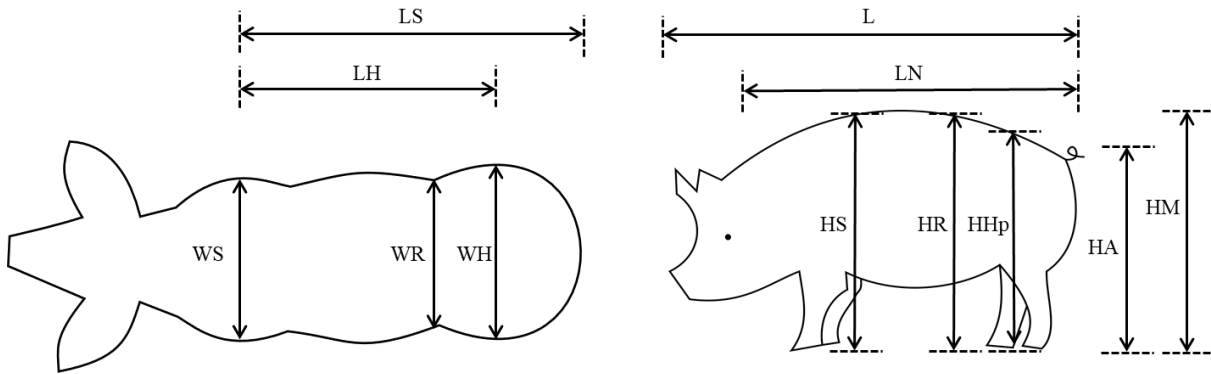

Figure 5. Dimensions acquired from top-view images: HA – average height, HM – maximum height, HS – height at shoulders, HR – height at last rib, HHp – height at hip, WS – width at shoulders, WR – width at last rib, WH – width at hip, LN – length from neck to rump, LS – length from shoulders to rump, LH – length from shoulders to hip, L – length, from snout to rump.
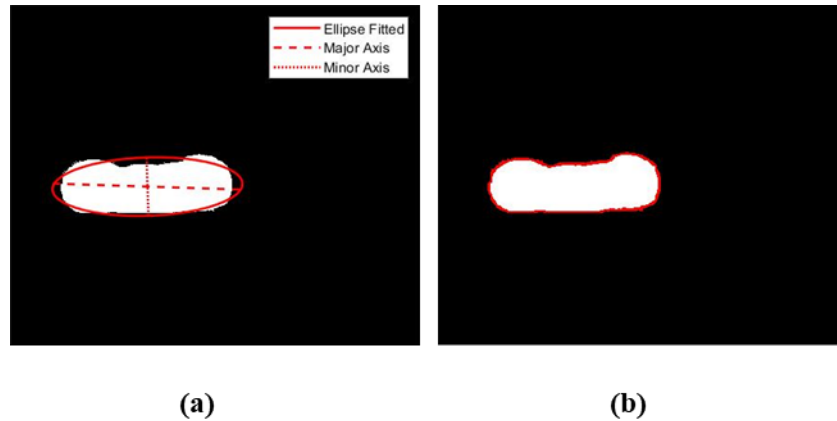
Figure 6. (a) Ellipse fitted on sows' body and major and minor axis of ellipse, and (b) perimeter of sow's body acquired.

At the last rib region, the length and angle (theta) of its curvature, formed by points P1 (lowest point to the left of curve), P2 (highest point of the curve), and P3 (lowest point to the right of the curve), were calculated (Figure 7). Also, the height (H) of the curvature was calculated between P3 and the average between P1 and P2. After that, a second-degree polynomial was fitted at the last rib curvature.

All dimensions were collected in pixel units, then, equation 1 was used for unit transformation from pixels to cm, and equation 2, also proposed on chapter 3 of this thesis, was used for unit transformation from px to cm².

The following regression models were trained and tested on a numerical computing software (MATLAB, version R2018a) to predict body condition score, backfat, and weight: linear regression, stepwise regression, support vector machine models (linear, quadratic, cubic, and gaussian), regression trees, and gaussian process regression. Eighty five percent of the data set was used for models' development and the remaining 15% was used for testing.

The variables tested for body condition score predictions were widths at shoulder (WS), last rib (WR), and hip (WH); major and minor axis of ellipse fitted on animal's body; and perimeter of animal's body; angle, height, length, and coefficient of the quadratic component of second-degree polynomial fitted on the curvature at last rib region. For backfat prediction, the variables tested were the same tested for body condition score, plus heights (maximum, average, at shoulders, at hip, and at last rib), lengths (from snout to rump, from neck to rump, from shoulders to rump, and from shoulders to hip), area and projected volume of the animal's body. For some of the animals it was not possible to acquire backfat, so a reduced number of animals was used for the regression.
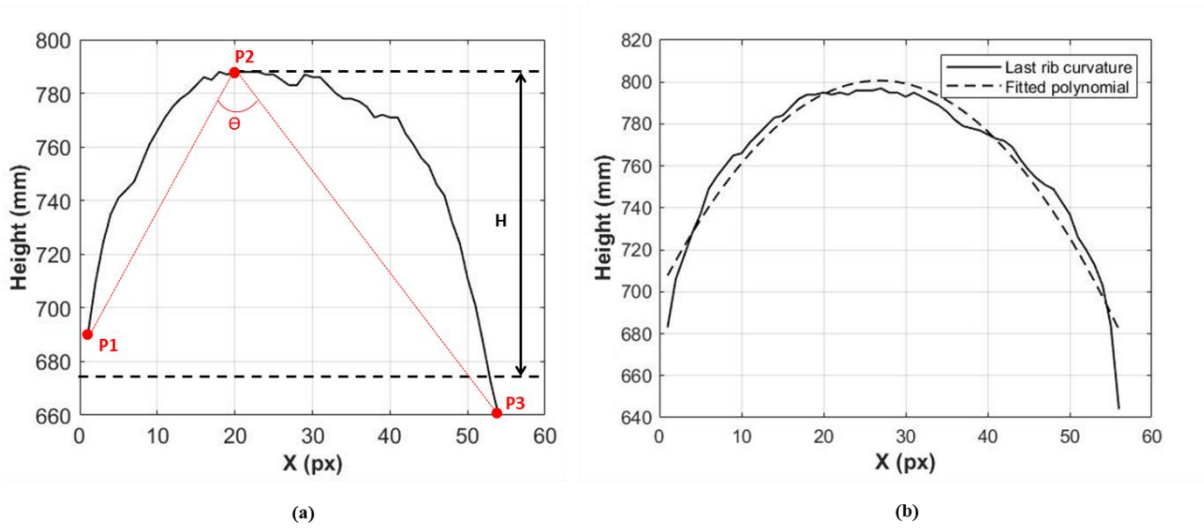
Figure 7. Curvature at last rib. Theta (θ) is the angle formed by points P1 (lowest point to the left), P2 (highest point), and P3 (lowest point to the right). The height (H) of the curvature is calculated between the P2 and the average between P1 and P3. (b) Second-degree polynomial fitted at last rib's curvature.

For weight prediction the variables tested were: area and projected volume of the animal's body, heights (maximum, average, at shoulders, at hip, and at last rib), widths (at shoulders, at hip, and at last rib) , lengths (from snout to rump, from neck to rump, from shoulders to rump, and from shoulders to hip), major and minor axis of ellipse fitted on animal's body; and perimeter of animal's body. For all models, principal component analysis was performed to select the variables that explained at least 95% of the variance of the predicted variable.

$$S_{cm^2} = S_{cm^2} \times 0.076 \times Z_m^{1.928} \tag{2}$$

where:

Scm^2 = area, in cm;

Spx = area, in pixels;

Zm = distance from the camera to the object being analyzed, in meters.

4.3 Results and Discussion

The preliminary results showed a high correlation (Figure 8) between width of the paper cylinder and body condition score (BCS), with an R^2 of 0.9792 and an average absolute error of 3.2%, or 0.47 units of BCS.

The body condition scores (BCS) of the population ranged from 8 to 19.5 units. The best model (smallest error and highest R^2) for predicting body condition score was a multiple linear regression found through the stepwise regression model, with form shown by eq. 3 and coefficients presented on Table 1. The selected inputs were the minor axis of the ellipse fitted around sow's body, the width at shoulders, and the angle, theta, of the last rib's curvature (Figures 9a, 9b, and 9c). The R^2 for this regression was 0.5175, with a standard error of 1.4659. The average absolute error of the model for the test set was 7.7%, or 1.0 unit of BCS. The R^2 of predicted versus actual BCS for the test set was 0.7769, with an intercept of 4.8094 and a slope of 0.6659 (Figure 9d).
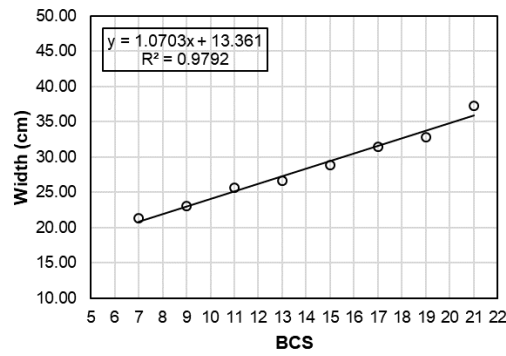
Figure 8. Width of paper cylinder, in cm, versus body condition score (BCS) obtained with caliper.

Previous results obtained by Kuzuhara et al. (2015) showed an R^2 of 0.73 for a multiple linear regression predicting BCS of cows that used as inputs six geodesic lines along the back of the animal and parity. The results obtained in the present work were slightly lower, but the animal differences in anatomy should be taken in consideration and the comparison should be done with reservations.

$$BCS = a + b \times MiA + c \times WS + d \times \theta \tag{3}$$

where:

BCS = body condition score;

MiA = length of minor axis of ellipse fitted around sow's body, in cm;

WS = width at shoulders, in cm;

θ = angle of last rib's curvature, in °;

a, b, c, d = coefficients.

The errors on the model could have been caused by different sources. One source could be human error, failing to consistently acquire the body condition score with the caliper due to animal's movement specially when the animals were in the group pens and had more range of movement.

Figure 10 shows the curvatures at last rib for two sows classified with a body condition score of 12. One sow was younger and pregnant (located in the group pen), while the other was an open sow located in an individual crate. It's easy to see that the curvature for both sows is different, with one animal being wider than the other. This difference could indicate either a measurement error or that the back curvature does not correlate so well with the calliper measurements. Knauer & Baitinger (2015) found a maximum correlation between BCS and caliper measurements of 0.76, indicating that, although a less subjective measurement of BCS is much needed, a perfect gold standard for this variable is still needed.
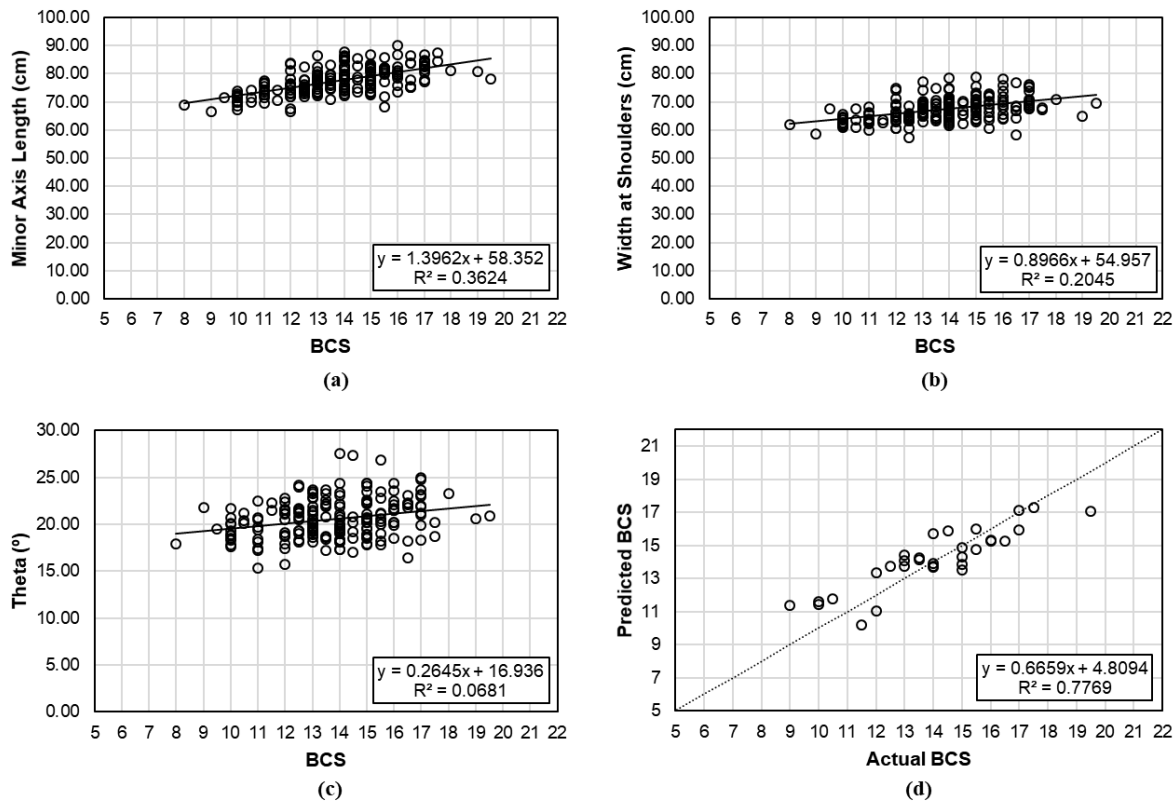
Figure 9. Variables selected for body condition score (BCS) prediction model plotted against BCS: length of minor axis of ellipse fitted around sow's body (a), width at shoulders (b), and angle, theta, of last rib's curvature (c). Predicted versus actual BCS for the test set are plotted on (d).
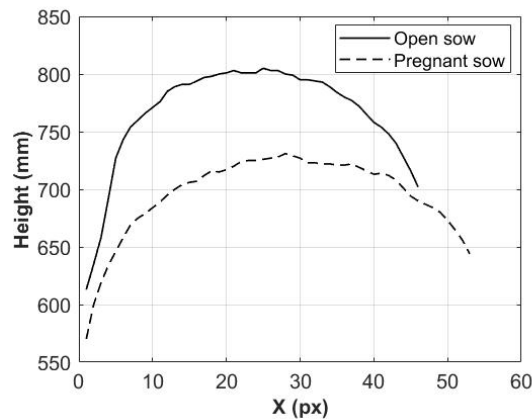

Figure 10. Curvature at last rib for two sows classified with a body condition score of 12. The shorter and wider sow (dashed line) was younger and pregnant.

The backfat (BF) of the population ranged from 8 to 30 mm. The best model (smallest error and highest R^2) for predicting backfat was a multiple linear regression found through the stepwise regression model, with form shown by eq. 4 and coefficients presented on Table 1. The selected inputs were the height of last rib's curvature, the perimeter of sow's body, the major axis of the ellipse fitted around sow's body, the length from snout to rump, and the predicted body condition score (using eq.3) (Figures 11a, 11b, 11c, 11d, and 11e). The R^2 for this regression was 0.4863, with a standard error of 3.5841. The average absolute error of the model for the test set was 16.07%, or 2.44

mm. The R² of predicted versus actual BF for the test set was 0.6650, with an intercept of 4.9429 and a slope of 0.6832 (Figure 11f). This value was smaller than the obtained by Weber et al. (2014) for backfat prediction from depth cameras for dairy cows (R² = 0.96), but, again, the animal differences in anatomy should be taken in consideration and the comparison should be done with reservations.

$$BF = a + b \times CH + c \times P + d \times MA + e \times L + f \times pBCS \qquad (4)$$

where:

BF = backfat, in mm;

CH = height of last rib's curvature, in cm;

P = perimeter of sow's body, in cm;

MA = length of major axis of ellipse fitted around sow's body, in cm;

L = length from snout to rump, in cm;

$pBCS$ = predicted body condition score;

a,b,c,d,e,f = coefficients.

Principal component analysis showed that the variable projected volume could explain 100% of the variance of the model (out of the variables tested) for predicting animal mass, so a simple linear regression of volume versus mass was performed (Figure 12a), with form presented in eq.4 and coefficients presented on Table 1. The R² for this regression was 0.8749, with a standard error of 9.9166. The average absolute error of the model for the test set was 3.8%, or 6.95 kg. This value is slightly smaller than the value obtained by Condotta et al. (2018) (4.6%) for predicting grow-finishing pigs' mass.

The R² of predicted versus actual body mass for the test set was 0.9321, with an intercept of 18.693 and a slope of 0.8979 (Figure 12b). This value is greater than the obtained (R² of 0.92) by Kashiha et al. (2014) for mass prediction of grow-finish pigs, but smaller than the values obtained by Kongsro (2014) for boars (R² = 0.99), by Condotta et al. (2018) (R² = 0.99) , and by Pezzuollo et al. (2018) (R² = 0.99) for grow-finishing pigs. This smaller R² obtained probably has to do with the smaller mass range of the animals, as for the greater error, it must be taken in consideration that sows have different anatomy from grow-finish pigs and boars, which can reduce the correlation between volume and mass.

Overall, the proposed method showed a satisfactory performance in the estimation of the three variables (body condition, backfat, and mass) assessed. Although the errors are, sometimes, slightly larger than errors obtained by other authors when analyzing these characteristics for other animals, the proposed method showed a promising way to assess the physical condition of sows in a fast, objective and non-invasive way, that can be automated. Problems with this approach are mainly related with the difficulty in having reliable gold standards for model development, especially for body condition. Next steps of this research should use more animals to validate the model, and test weight prediction in pregnant sows.
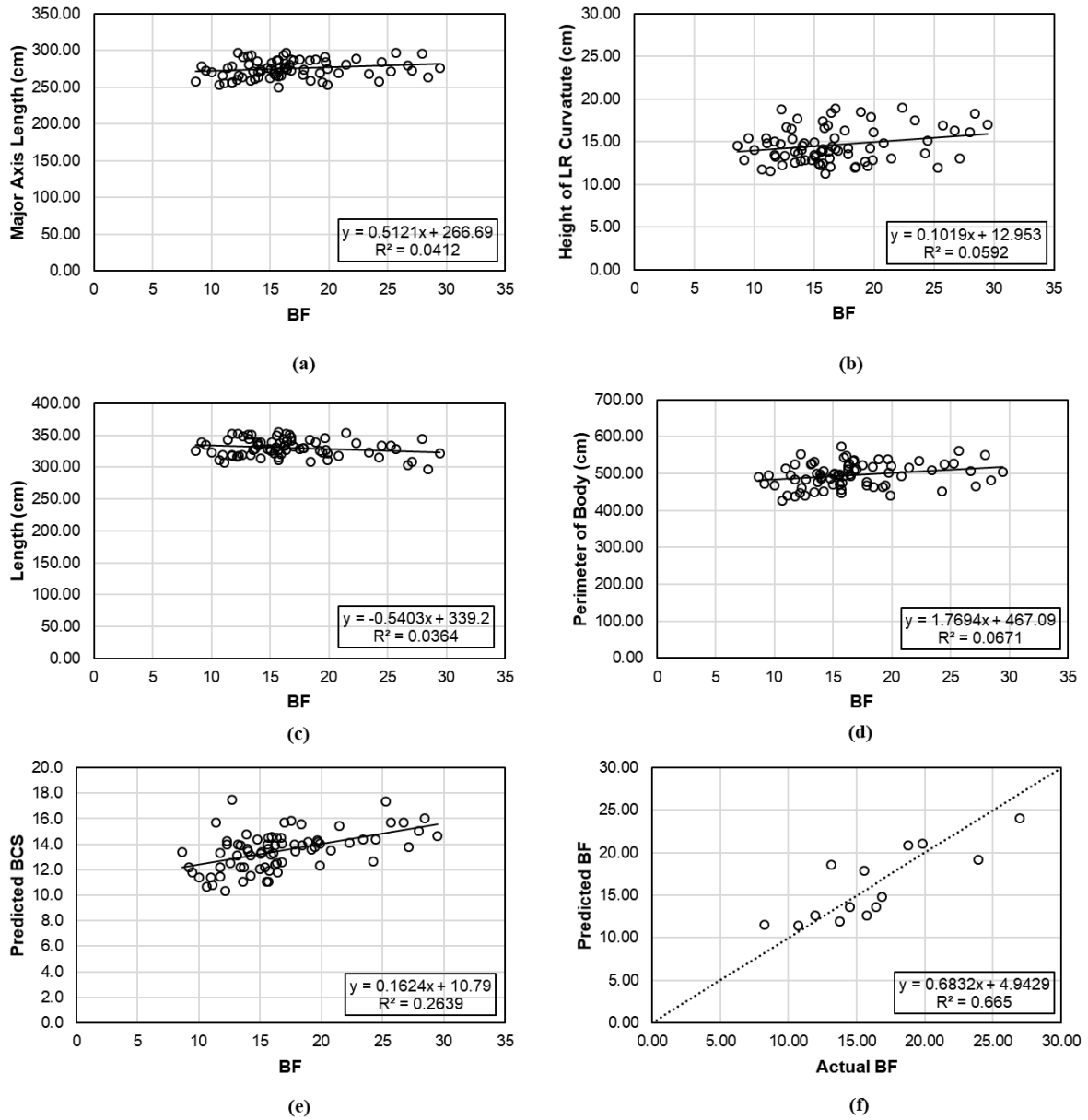
Figure 11. Variables selected for backfat (BF) prediction model plotted against BF: length of major axis of ellipse fitted around sow's body (a), height of last rib's curvature (b), length from snout to rump (c), perimeter of sow's body (d), and predicted BCS (e). Predicted versus actual BF for the test set are plotted on (f).

$$M = a + b \times V \qquad\qquad (5)$$

where:

M = body mass, in kg;

V = projected volume, in cm³;
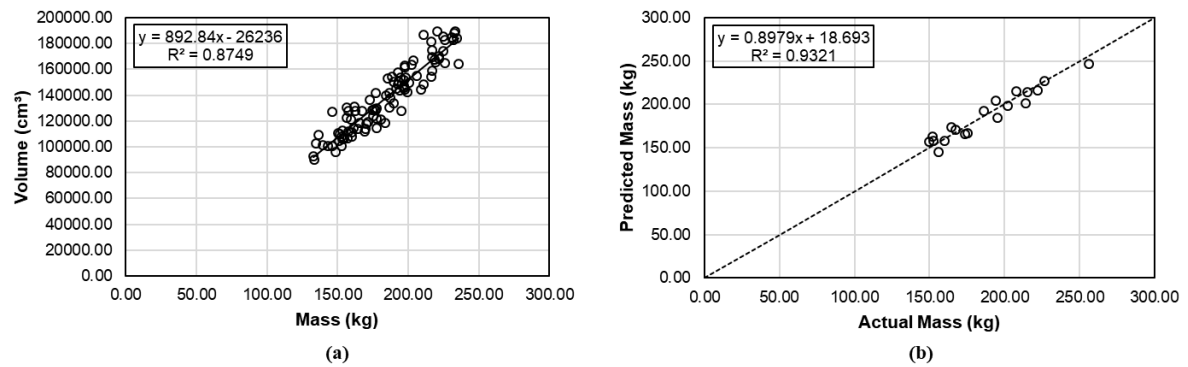
a, b = coefficients.

Figure 12. (a) Projected volume versus body mass. (b) Predicted versus actual mass.

Table 1. Regression coefficients for body condition score (BCS), backfat (BF), and mass predictions.

Regression	Coefficients						R^2
	a	**b**	**c**	**d**	**e**	**f**	
BCS	-14.7036	0.3259	-0.0715	0.3874	-	-	0.5175
BF	25.2855	0.0389	0.0505	0.0359	-0.2036	1.4117	0.4863
Mass	48.7898	0.0010	-	-	-	-	0.8749

Table 2. Regression statistics for body condition score (BCS), backfat (BF), and mass predictions.

Regression Statistics	BCS	BF	Mass
R^2	0.5175	0.4863	0.8749
Standard Error	1.4659	3.5841	9.9166
Number of Observations	191	75	96

4.4 Conclusions

Regression models were performed to obtain body condition score, backfat, and body mass from variables obtained with a commercially available depth camera. A multiple linear regression was obtained using the minor axis of the ellipse fitted around sow's body, the width at shoulders, and the angle, of the last rib's curvature to predict BCS. To predict backfat, a multiple linear regression was performed using the height of last rib's curvature, the perimeter of sow's body, the major axis of the ellipse fitted around sow's body, the length from snout to rump, and the predicted body condition score. It was possible to obtain the body mass with a simple linear regression using the projected volume of the sows' body. With these three characteristics it could be possible to have better insights on the physical condition of sows and aid on better and faster management decisions.

References

Charette, R., Bigras-Poulin, M., & Martineau, G. P. (1996). Body condition evaluation in sows. Livestock Production Science, 46(2), 107–115. https://doi.org/10.1016/0301-6226(96)00022-X

Condotta, I. C. F. S., Brown-Brandl, T. M., Silva-Miranda, K. O., & Stinn, J. P. (2018). Evaluation of a depth sensor for mass estimation of growing and finishing pigs. Biosystems Engineering, 2–9. https://doi.org/10.1016/j.biosystemseng.2018.03.002

De Rensis, F., Gherpelli, M., Superchi, P., & Kirkwood, R. N. (2005). Relationships between backfat depth and plasma leptin during lactation and sow reproductive performance after weaning. Animal Reproduction Science, 90(1–2), 95–100. https://doi.org/10.1016/j.anireprosci.2005.01.017

Eissen, J. J., Kanis, E., & Kemp, B. (2000). Sow factors affecting voluntary feed intake during lactation. Livestock Production Science, 64(2–3), 147–165. https://doi.org/10.1016/S0301-6226(99)00153-0

Esbenshade, K. L., Britt, J. H., Armstrong, J. D., Toelle, V. D., & Stanislaw, C. M. (1986). Body condition of sows across parities and relationship to reproductive performance. Journal of Animal Science, 62(5), 1187–1193. https://doi.org/10.2527/jas1986.6251187x

Kashiha, M., Bahr, C., Ott, S., Moons, C. P. H., Niewold, T. A., Ödberg, F. O., & Berckmans, D. (2014). Automatic weight estimation of individual pigs using image analysis. Computers and Electronics in Agriculture, 107, 38–44. https://doi.org/10.1016/j.compag.2014.06.003

Kim, K. H., Hosseindoust, A., Ingale, S. L., Lee, S. H., Noh, H. S., Choi, Y. H., … Chae, B. J. (2016). Effects of gestational housing on reproductive performance and behavior of sows with different backfat thickness. Asian-Australasian Journal of Animal Sciences, 29(1), 142–148. https://doi.org/10.5713/ajas.14.0973

Knauer, M., Stalder, K., Baas, T., Johnson, C., & Karriker, L. (2012). Physical Conditions of Cull Sows Associated with On-Farm Production Records. Open Journal of Veterinary Medicine, 02(03), 137–150. https://doi.org/10.4236/ojvm.2012.23023

Knauer, M., Stalder, K. J., Karriker, L., Baas, T. J., Johnson, C., Serenius, T., … McKean, J. D. (2007). A descriptive survey of lesions from cull sows harvested at two Midwestern U.S. facilities. Preventive Veterinary Medicine, 82(3–4), 198–212. https://doi.org/10.1016/j.prevetmed.2007.05.017

Knauer, M. T., & Baitinger, D. J. (2015). The sow body condition caliper. Applied Engineering in Agriculture, 31(2), 175–178. https://doi.org/10.13031/aea.31.10632

Kongsro, J. (2014). Estimation of pig weight using a Microsoft Kinect prototype imaging system. Computers and Electronics in Agriculture, 109, 32–35. https://doi.org/10.1016/j.compag.2014.08.008

Kuzuhara, Y., Kawamura, K., Yoshitoshi, R., Tamaki, T., Sugai, S., Ikegami, M., … Yasuda, T. (2015). A preliminarily study for predicting body weight and milk properties in lactating Holstein cows using a three-dimensional camera system. Computers and Electronics in Agriculture, 111, 186–193. https://doi.org/10.1016/j.compag.2014.12.020

Maes, D. G. D., Janssens, G. P. J., Delputte, P., Lammertyn, A., & De Kruif, A. (2004). Back fat measurements in sows from three commercial pig herds: Relationship with reproductive efficiency and correlation with visual body condition scores. Livestock Production Science, 91(1–2), 57–67. https://doi.org/10.1016/j.livprodsci.2004.06.015

Magowan, E., & McCann, M. E. E. (2006). A comparison of pig backfat measurements using ultrasonic and optical instruments. Livestock Science, 103(1–2), 116–123. https://doi.org/10.1016/j.livsci.2006.02.002

Patience, J. F., & Thacker, P. A. (1989). Swine nutrition guide (No. 636.4 P2737s Ej. 1 009811). University of Saskatchewan.

Pezzuolo, A., Guarino, M., Sartori, L., González, L. A., & Marinello, F. (2018). On-barn pig weight estimation based on body measurements by a Kinect v1 depth camera. Computers and Electronics in Agriculture, 148(August 2017), 29–36. https://doi.org/10.1016/j.compag.2018.03.003

Phillips, R. W., & Dawson, W. M. (1936). A study of methods for obtaining measurements of swine. Journal of Animal Science, 1936(1), 93-99.

Quality, W. (2009). Welfare Quality® assessment protocol for pigs (sows and piglets, growing and finishing pigs). Welfare Quality® Consortium, Lelystad, the Netherlands.

Salak-Johnson, J. L., Niekamp, S. R., Rodriguez-Zas, S. L., Ellis, M., & Curtis, S. E. (2007). Space allowance for dry, pregnant sows in pens: Body condition, skin lesions, and performance. Journal of Animal Science, 85(7), 1758–1769. https://doi.org/10.2527/jas.2006-510

Schofield, C. P., Marchant, J. A., White, R. P., Brandl, N., & Wilson, M. (1999). Monitoring pig growth using a prototype imaging system. Journal of Agricultural and Engineering Research, 72(3), 205–210. https://doi.org/10.1006/jaer.1998.0365

Sell-Kubiak, E. (2015). Non-genetic variance in pigs: genetic analysis of production and reproduction traits.

Weber, A., Salau, J., Haas, J. H., Junge, W., Bauer, U., Harms, J., … Thaller, G. (2014). Estimation of backfat thickness using extracted traits from an automatic 3D optical system in lactating Holstein-Friesian cows. Livestock Science, 165(1), 129–137. https://doi.org/10.1016/j.livsci.2014.03.022

Wu, J., Tillett, R., McFarlane, N., Ju, X., Siebert, J. P., & Schofield, P. (2004). Extracting the three-dimensional shape of live pigs using stereo photogrammetry. Computers and Electronics in Agriculture, 44(3), 203–222. https://doi.org/10.1016/j.compag.2004.05.003

Zaragoza, L. E. O. (2009). Evaluation of the accuracy of simple body measurements for live weight prediction in growing-finishing pigs. MSc. Diss. Univ. of Illinois, Urbana, Illinois.

5 IMPROVING SOWS' PERFORMANCE: LAMENESS DETECTION THROUGH DEPTH IMAGE ANALYSIS

Abstract

To maintain the animal welfare and production in appropriate standards it is necessary to observe, control and maintain the physical condition of sows in acceptable levels. Currently, the classification of lameness is done by subjective methods, thus is dependent on the opinion of the manager, which can generate differences between ratings. As alternatives to these subjective methods of classification, various methods have been proposed to obtain a more objective measure. A way to standardize these measurements would be to automate the process by analyzing images generated by depth cameras. The present work aimed to propose a method for early detection of lameness in sows, adapting the kinematics method to be used with depth cameras and without the use of reflective markers. Three models presented the best accuracy (76.9%): linear discriminant analysis, fine 1-nearest neighbor, and weighted 10-nearest neighbors. The input variables used on the models were obtained from depth videos (number, time, and length of steps for each of the four regions analyzed - left and right shoulders and left and right hips; total walk time; and number of local maxima for head region). With the automation of lameness detection, it could be possible to have better insights on the physical condition of sows and aid on better and faster management decisions.

Keywords: Precision livestock farming; Time-of-flight; Swine

5.1 Introduction

To maintain the animal welfare and production in appropriate standards it is necessary to observe, control and maintain the physical condition of sows in acceptable levels. The animal welfare assessment protocol for pigs, Welfare Quality® (Quality, 2009), states that good health, one of the principles of the animal welfare, is composed of three criteria: absence of injury, absence of disease and absence of pain induced by manager. It is proposed to evaluate the first criterion on sows by verifying the presence of lameness.

Lameness causes pain and difficulty of locomotion (Anil et al., 2009) and, however, it is a common disorder in sows that causes negative impacts in both welfare and production, since the animals that demonstrate this problem, have a smaller number of born-alive piglets, fewer gestations per year and are removed from the herd at a younger age than the ideal (Anil et al., 2009). It is suggested (Quality, 2009) to classify lameness in a subjective method, by visually rating the animals in three levels: level 0 (normal gait, or animal with difficulty on walking, but still using all four legs), level 1 (sow severely lame, with asymmetric walking) and level 2 (animal cannot support any weight on affected limb, or cannot walk).

As alternatives, various methods have been proposed to obtain a more objective measurement of lameness. Kinetics and kinematics have been widely used in horses and cows and they began to be used in pigs. The kinetics aims to relate the movement of the bodies with their causes and considers the dynamic forces and acceleration. The footprint was analyzed in many species to study locomotion disorders. One of the possibilities of kinetics is to study simultaneously the positioning of four legs and quantify parameters that cannot be measured with kinematics, such as slips when walking, trodden angles and the area of limbs in contact with the floor (Nalon et al., 2013). The use of a hallway with floor covered in clay has been tested for acquiring the footprints of sows (Grégoire et al., 2013), but it has not been possible to establish a relationship between the footprint pattern and the degree of lameness, perhaps because of the floor type used.

Kinematic analysis quantifies the characteristics of the animal's gait in the form of measures related with time, distance, and angles that describe the movements of the body segments and the joint angles. This analysis is made using reflective markers in predetermined locations on the body of the animal and video recording of the gait.

With this technique, several parameters can be simultaneously analyzed by an auto-tracking software, however, some problems have been associated with it, mainly related with the placing of markers and their movement with the walk, the difficulty in finding joints or bones located behind muscle and fat where these markers are positioned, and repeatability of positioning (Nalon et al., 2013). Despite the problems, this method was effective to show (Grégoire et al., 2013) that lame sows have lower walking speed, spend less time standing during a period of 24 hours and tend to step more often during the time following the feeding.

An attempt was made (Stavrakakis et al., 2015) to reduce costs with the kinetics method by using a commercial depth camera to detect vertical position trajectories of a dorsal neck marker on pigs. It was observed that the information obtained by the depth cameras is suitable to track characteristics of walking in pigs based on neck elevation (errors ranged from 0.5 to 2.0 cm when compared to the reflective markers method), showing potential to be used in the detection and classification of lameness, eliminating both the problem with the placement of the markers and the costs involved in the process.

Another method used (Meijer et al, 2014) for lameness detection is the use of a pressure mat. With this method it is possible to detect the standard gait of a non-lame pig. This information can be used to detect an abnormal gait, indicating a lame pig. It was shown (Meijer et al, 2014) that the gait of a lame pig is asymmetric, and this can be detected with a pressure mat.

This manuscript aimed to propose a method for early detection of lameness in sows, adapting the kinematics method to be used with depth cameras and without the use of reflective markers.

5.2 Materials and Methods

The experiment was conducted in a gestating building of the U.S. Meat Animal Research Center, from the Agriculture Research Service-ARS of United States Department of Agriculture – USDA (-98.13° W, 42.52° N). Animal digital and depth images were collected on a population of sows at four parities, and at two different time-points: on the day of moving to the farrowing building and on the day of moving from the farrowing building. All animal procedures were performed in compliance with federal and institutional regulations regarding proper animal care practices (FASS, 2010).

5.2.1 Animal Specifics

Two-hundred and twenty-eight sows at four different parities (1, 2, 3, and 4), weighing approximately between 130 and 260 kg, from a rotational Landrace and Yorkshire cross were sampled. The animals were allocated in a gestating building. Animals were sampled at two different time-points: on the day of moving to the farrowing building and on the day of moving from the farrowing building. The first group received a restricted diet and ad libitum water and were housed in a group-pen; while the second group had ad libitum access to both feed and water and were housed in individual crates. Diets were a mix of corn and soybean meal formulated to meet or exceed National Research Council recommendations (NRC, 2012).

5.2.2 Data Acquisition

Microsoft® Kinect Studio program was used to acquire both digital RGB color and depth videos from a commercially available depth camera (Microsoft Kinect® v.2). The program was deployed on a Windows®-based computer for data collection. The camera was positioned above the hallway of the building mounted on the ceiling to take both dorsal color (1920 x 1080 pixels per frame, Figure 1a) and depth videos (512 x 424 pixels per frame, Figure 1b) of the animals while being moved to and from the farrowing building, at approximately 30 frames per second.
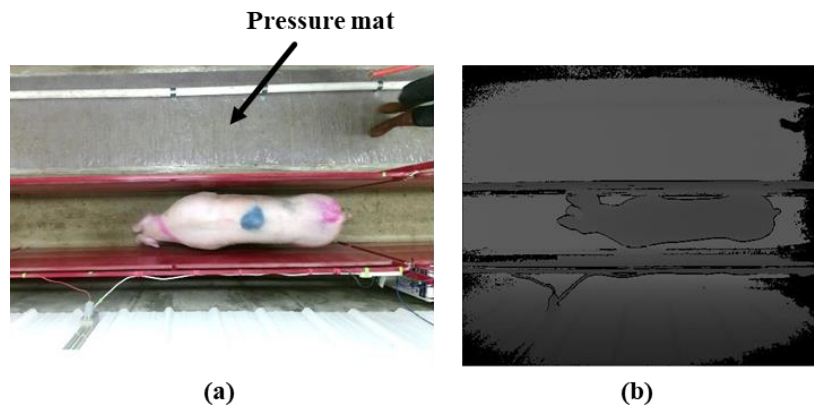

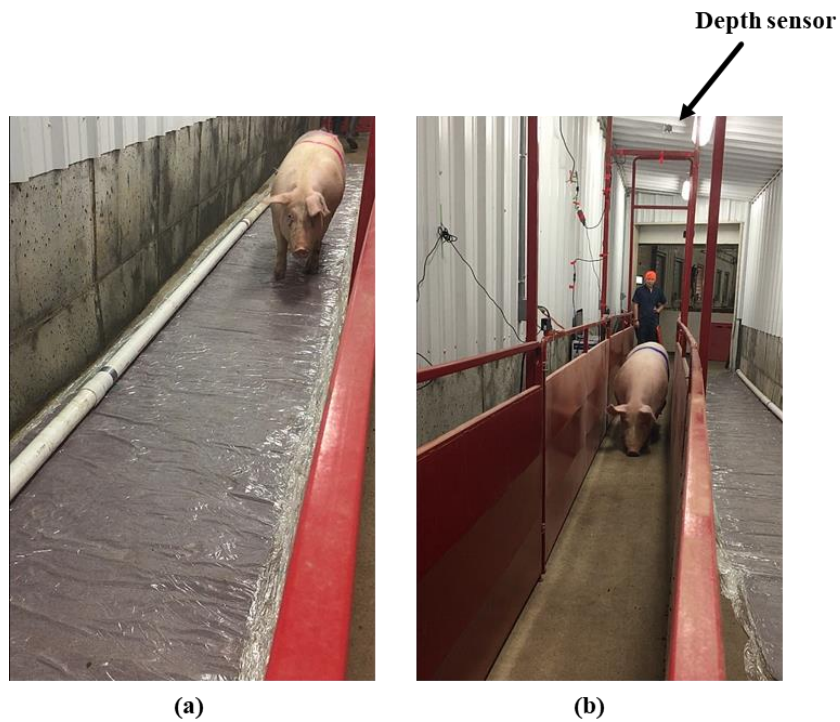**Figure 1.** Top-view of the experiment setting. (a) Color and (b) depth frames acquired.

Figure 2. Experiment settings. (a) Animal walking on pressure mat. (b) Walkway with depth camera mounted on ceiling.

Animals were weighed using a Rice Lake weighing Systems digital weighing scale, that was calibrated by the company and regularly checked with a 50 lb. weight. The lameness level of the animals was visually assessed, validated with a commercially available pressure mat (GAITFour® Walkway, Figures 1a and 2a).

The assessment classified animals in lame or not lame, and, in case of lame, the animals were classified in one of two lameness categories: mild (animal with difficulty on walking, but still using all four legs), or severe (asymmetric walking). No animals with extremely severe lameness (e. g. animal cannot support any weight on affected limb or cannot walk) were observed on the population.

For the pressure mat evaluation, sows individually walked across the mat and the data was deployed on a laptop using the GAITFour® software. In case the walk was not usable (e.g. animal backed up, or stepped outside the mat with one or more limbs), the animals were walked across the mat again, up to two repetitions.

5.2.3 Data Analysis

An algorithm, proposed by Condotta et al. (2018), was used in a numerical computing software (MATLAB, version R2018a) for pre-processing the images. After that, the animal's head region was selected by applying a circular binary mask on the image, starting from the shoulder, with diameter equal to the width at the shoulders of the animal. The rest of the sow's body was segmented in halves (left and right side), and for each side the regions of shoulders and hips were selected (Figure 3). For each of the four regions (head, shoulder - left and right, and hip – left and right), the centroid was calculated. Also, position (x, and y directions) and height at the centroids was acquired. Average, maximum, and minimum height at each region was recorded. The animal's velocity was also measured by calculating the Euclidian distance between the positions of the animals' centroid (not considering its head) over the elapsed time between frames.
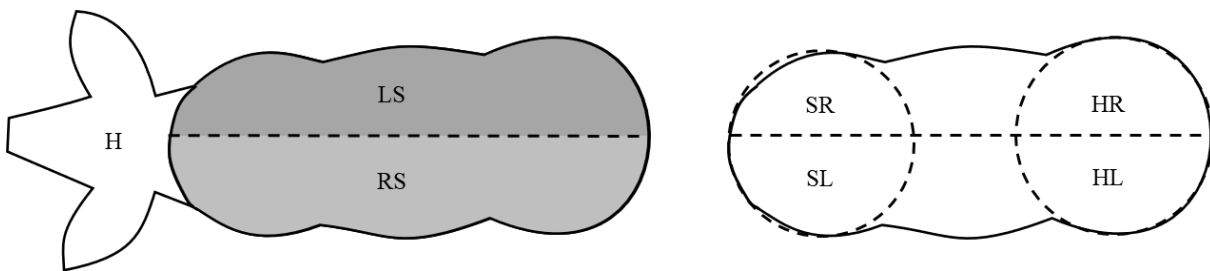

Figure 3. Regions selected of the animal body: head (H), left (LS) and right sides (RS), shoulders (left - SL and right - SR sides), and hip (left - HL and right - HR sides).

The curves of height by time obtained for the centroids of all five regions were plotted and analyzed (Figure 4a). For that, an algorithm was developed on a numerical computing software (MATLAB, version R2018a) that smoothed the curves using a moving average filter, then found the local maxima of the curves. For the shoulders and hips regions, the local maxima were marked as being the steps of the animals. This information was validated by plotting curves for left and right sides together (Figure 4b) and finding the number of times that the curves crossed each other. The mode of all 6 number of steps obtained (one for each region, plus two for both shoulders and both hips) as being the number of steps of the animals. Time and length for each step was recorded.

The following classification models were trained and tested on a numerical computing software (MATLAB, version R2018a) to predict lameness level: decision tress, discriminant analysis, support vector machines,

and nearest neighbor classifiers. To evaluate the models' performance in making predictions on new datasets that it has not been trained on and prevent overfitting during training, a five-fold cross-validation was performed. The input variables used were: number, time, and length of steps for each of the four regions analyzed (left and right shoulders, and left and right hips), total walk time, and number of local maxima for head region.
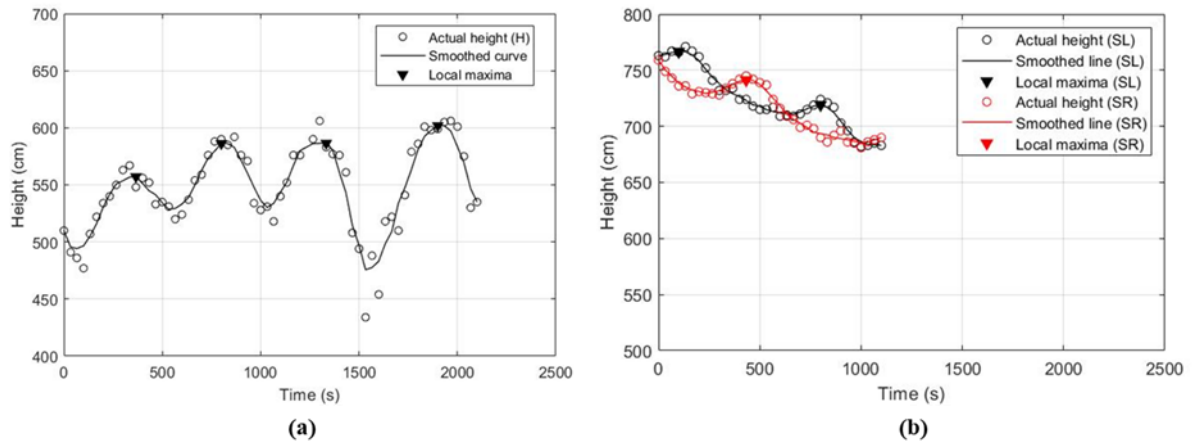

Figure 4. Curves of height versus time for the head (H) region and the shoulders regions - left (SL) and right (SR). Smoothed curves and local maxima are also plotted.

5.3 Results and Discussion

Nine sows of the population presented a lameness level of 2 (severe), and eight animals presented a lameness level of 1 (mild). For training the classification models, nine non-lame animals (level 0) were randomly selected. Table 1 presents the accuracy for all models tested. The three models that presented highest accuracy for predicting lameness level were: (1) linear discriminant analysis (Fisher discriminant – Fisher, 1936), that assumes that different classes generate data based on different Gaussian distributions; (2) fine nearest neighbor classifier, with 1 nearest neighbor used to classify each point during prediction and no distance weighing; and (3) weighted nearest neighbor classifier, with 10 nearest neighbors and squared inverse distance weighting function (the weight is $1/distance^2$). The distance metric used for both nearest neighbors' models was the Euclidean distance.

The accuracy of all three best models was 76.9%, with 62.5% of true positive rate for the mild lameness level, 66.7% of true positive rate for the severe lameness level, and 100% of true positive rate for the non-lame level. Confusion matrixes with these results are presented on Figure 5. All miss-classifications were of lame animals (either severe or mild) classified as not-lame (false negatives), which is the least ideal error. Jabbar et al. (2017) found an accuracy of 95.0% for lameness detection in dairy cows with two prediction levels, lame and not-lame. Van Hertem et al. (2014) obtained correct classification rate of 53.0% for dairy cows at five lameness levels, and 81.2% when using a binary classification (lame versus not-lame).

Although the accuracy obtained in this study is slightly smaller than some of the previous results obtained for dairy cows, the animal differences in anatomy should be taken in consideration and the comparison should be done with reservations. Van Hertem et al. (2014) found that consecutive measurements on the same animal can improve the classification output of a computer vision system, so this is something that could be tested on future steps of this research, aiming the improvement on accuracy.

Table 1. Models tested to predict lameness level of sows and their accuracy.

Method	Model Type	Accuracy (%)
	Fine Tree	73.1
Decision Trees	Medium Tree	73.1
	Coarse Tree	73.1
Discriminant Analysis	Linear Discriminant	76.9
	Linear SVM	57.7
Support Vector Machines (SVM)	Quadratic SVM	65.4
	Cubic SVM	65.4
	Fine KNN	76.9
	Medium KNN	50.0
	Coarse KNN	46.2
Nearest Neighbour Classifiers (KNN)	Cosine KNN	46.2
	Cubic KNN	46.2
	Weighted KNN	76.9

Figure 5. Confusion matrix of predicted lameness level versus actual lameness level (0 – not lame, 1 – mildly lame, 2 – severely lame) for the three models with highest accuracy: linear discriminant analysis (a), fine nearest neighbor (b), and weighted nearest neighbor (c).

With the analysis of the graphs of height versus time obtained (Figures 7,8, and 9), it is possible to observe that lame animals take more time to walk the same distance (lower velocity), as previously shown by Grégoire et al. (2013). It was also possible to see that lame animals have smaller steps, so they take more steps to walk the same distance as non-lame animals. These facts were confirmed by the pressure mat analysis (Figure 6). The affected limb of lame animals presented a higher total press and a lower "down" time when compared with the non-affected limbs. They also have a higher number of head swings. The higher the lameness level, the higher the amplitude (Figure 7) of these swings. This could indicate that these animals use the head as a counter-balance of the affected limb.

Because a low number of animals on the population analyzed were classified as lame (17 out of 228, or 7.42%), future steps of this research should use more lame animals per level in order to improve the model. Overall, the results suggest that an accurate lameness detection can be done by applying a commercially available depth camera and a weighted 10-nearest neighbor classification model, with the possibility of automation on farm settings. The model should be improved using a higher number of animals to train the model. With this, it could be possible to have better insights on the physical condition of sows and aid on better and faster management decisions.
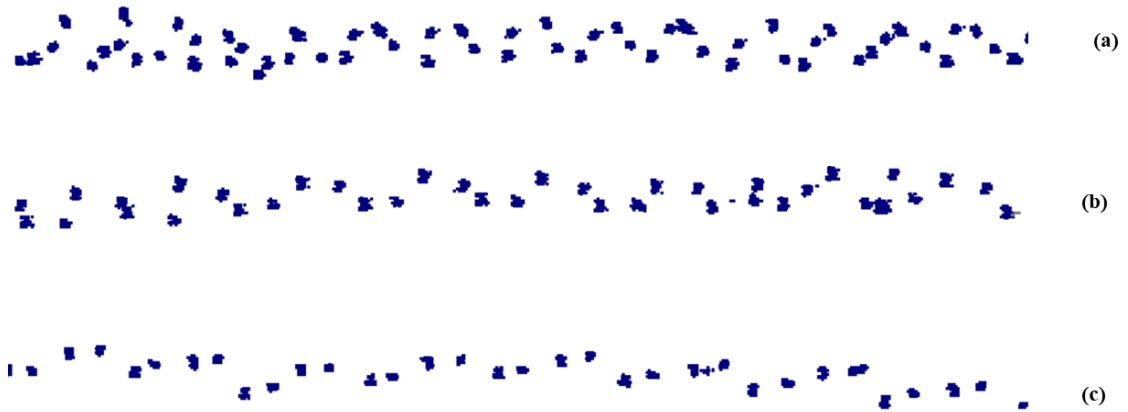
Figure 6. Steps of a severe lame (a) animal, a mildly lame (b) animal, and a non-lame (c) animal recorded by a pressure mat. The higher the lameness level, the higher the number of steps and the shorter the step.
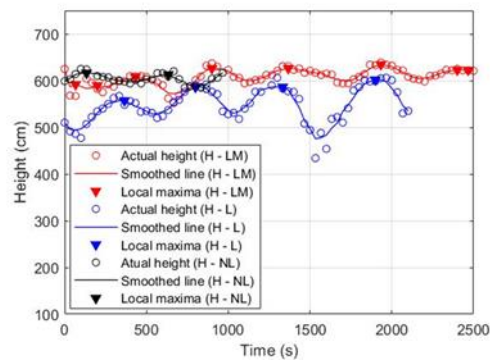

Figure 7. Curves of height versus time for head (H) region of a non- lame (NL), a mildly lame (LM), and a lame (L) sow.
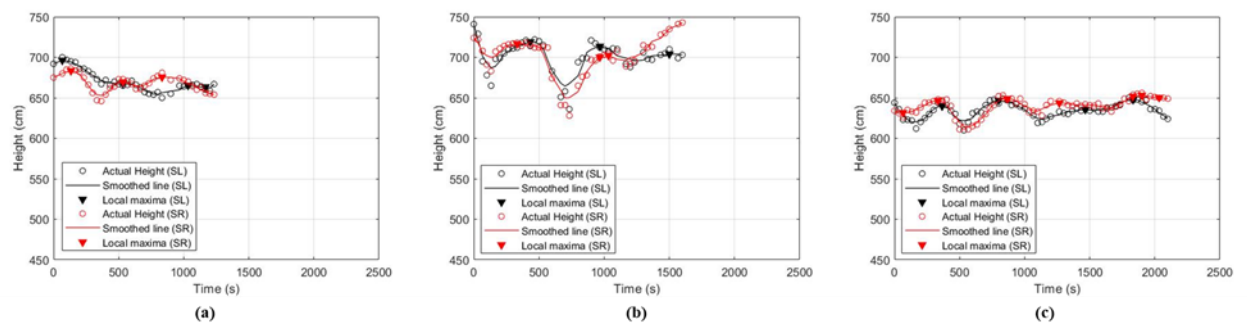

Figure 8. Curves of height versus time for the shoulders (left – SL, and right - SR) of a non- lame (a), a mildly lame (b), and a lame (c) sow.
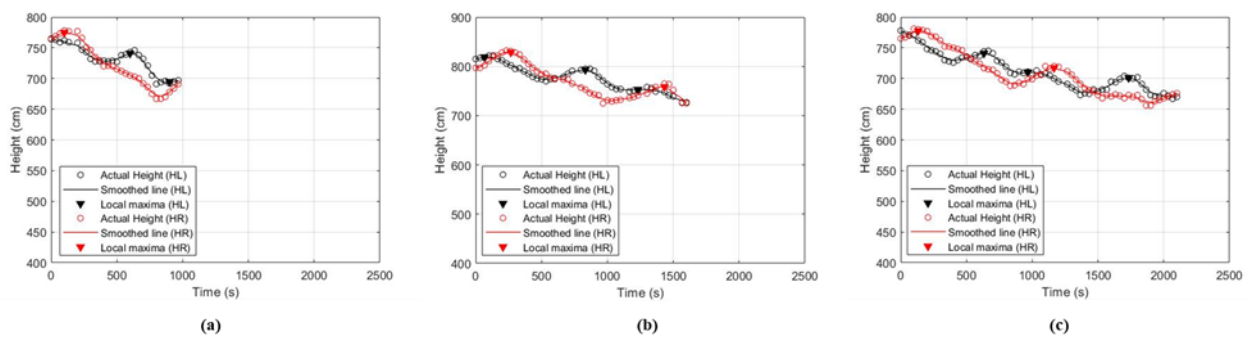
Figure 9. Curves of height versus time for the hips (left – HL, and right - HR) of a non- lame (a), a mildly lame (b), and a lame (c) sow.

5.4 Conclusions

A method for early detection of lameness in sows was proposed by using commercially available depth cameras and one of the three models: linear discriminant analysis, fine 1-nearest neighbor, and weighted 10-nearest neighbors. The input variables to the models were number, time, and length of steps for each of the four regions analyzed (left and right shoulders and left and right hips); total walk time; and number of local maxima for head region. The lameness can be classified with a good accuracy (76.9%). Future steps of this research should use more animals per level in order to improve the model. With the automation of lameness detection, it could be possible to have better insights on the physical condition of sows and aid on better and faster management decisions.

References

Anil, S. S., Anil, L., & Deen, J. (2009). Effect of lameness on sow longevity. Journal of the American Veterinary Medical Association, 235(6), 734-738.

Condotta, I. C. F. S., Brown-Brandl, T. M., Silva-Miranda, K. O., & Stinn, J. P. (2018). Evaluation of a depth sensor for mass estimation of growing and finishing pigs. *Biosystems Engineering*, 2–9. https://doi.org/10.1016/j.biosystemseng.2018.03.002

Fisher, R. A. The Use of Multiple Measurements in Taxonomic Problems. Annals of Eugenics, Vol. 7, pp. 179–188, 1936. Available at https://digital.library.adelaide.edu.au/dspace/handle/2440/15227.

Grégoire, J., Bergeron, R., D'Allaire, S., Meunier-Salaün, M.-C., & Devillers, N. (2013). Assessment of lameness in sows using gait, footprints, postural behaviour and foot lesion analysis. *Animal*, *7*(07), 1163–1173. https://doi.org/10.1017/s1751731113000098

Jabbar, K. A., Hansen, M. F., Smith, M. L., & Smith, L. N. (2017). Early and non-intrusive lameness detection in dairy cows using 3-dimensional video. *Biosystems engineering*, 153, 63-69. https://doi.org/10.1016/j.biosystemseng.2016.09.017

Meijer, E., Oosterlinck, M., van Nes, A., Back, W., & van der Staay, F. J. (2014). Pressure mat analysis of naturally occurring lameness in young pigs after weaning. BMC veterinary research, 10(1), 193.

Nalon, E., Conte, S., Maes, D., Tuyttens, F. A. M., & Devillers, N. (2013). Assessment of lameness and claw lesions in sows. *Livestock Science*, *156*(1–3), 10–23. https://doi.org/10.1016/j.livsci.2013.06.003

Quality, W. (2009). Welfare Quality® assessment protocol for pigs (sows and piglets, growing and finishing pigs). Welfare Quality® Consortium, Lelystad, the Netherlands.

Stavrakakis, S., Li, W., Guy, J. H., Morgan, G., Ushaw, G., Johnson, G. R., & Edwards, S. A. (2015). Validity of the Microsoft Kinect sensor for assessment of normal walking patterns in pigs. *Computers and Electronics in Agriculture*, *117*, 1–7. https://doi.org/10.1016/j.compag.2015.07.003

Van Hertem, T., Viazzi, S., Steensels, M., Maltz, E., Antler, A., Alchanatis, V., ... & Berckmans, D. (2014). Automatic lameness detection based on consecutive 3D-video recordings. *Biosystems Engineering*, 119, 108-116. https://doi.org/10.1016/j.biosystemseng.2014.01.009